CUP-SHAPED COTYLEDON2 activates *MIR319C* transcription and promotes cell proliferation in Arabidopsis leaf primordia

Naveen Shankar[1#], Abhishek Gupta[1], Somsree Roy[1], Vishwadeep Mane[1], Olivier Hamant[2] and Utpal Nath[1*]

1 Department of Microbiology and Cell Biology, Indian Institute of Science, Bengaluru, India.
2 Laboratoire de Reproduction et Développement des Plantes, Université de Lyon, ENS de Lyon, UCBL, INRA, CNRS, 46 Allée d'Italie, 69364 Lyon Cedex 07, France.
Current address: Department of Plant Physiology, Umeå Plant Science Centre, Umeå University, 901 87 Umeå, Sweden.

*Corresponding author. Email: utpalnath@iisc.ac.in

Abstract

The microRNA miR319 regulates leaf shape and size in diverse plant species by reducing the level of the target transcripts that encode JAW-TCP proteins, the transcription factors (TF) which commit the proliferating pavement cells to differentiation. Expression of *MIR319C*, one of the three miR319-producing genes in Arabidopsis, is expressed throughout the incipient leaf primordia, and the expression domain gets restricted to the base at later stages, partly due to the direct action of JAW-TCPs. However, the factors that activate and maintain *MIR319C* expression in leaf primordia are yet unknown. Here, we report the CUP-SHAPED COTYLEDON2 (CUC2) transcription factor as a direct activator of *MIR319C* transcription. In a yeast one-hybrid (Y1H) screen, we identified several NAC domain TFs as potential regulators of *MIR319C*. Subsequent ex vivo binding and transactivation assays suggested that CUC2 may bind to distal promoter region of *MIR319C*. Mutants with compromised *CUC2* and *MIR319C* activities exhibited smaller leaf areas and reduced pavement cell numbers due to early cell proliferation-to-differentiation transition. Morphometric analysis of higher order *CUC2* and *MIR319* loss-of-function mutants highlighted the crucial role of the *CUC2-MIR319* module in promoting leaf cell proliferation and indicated functional redundancy among the three *MIR319* genes in regulating JAW-TCP levels during leaf growth. Additionally, the phenotypes of mutants with altered *CUC2* and *MIR319/JAW-TCP* activities demonstrated that *CUC2* enhances leaf size through the *MIR319C-JAW-TCP* pathway. Overall, our findings uncovered a novel role for CUC2 in promoting cell proliferation by activating *MIR319C* transcription in the leaf primordia.

Introduction

Leaf development can be empirically divided into three major stages, namely initiation, primary morphogenesis, and secondary morphogenesis (Bar and Ori, 2014). Initiation of a leaf primordium commences with the specification of a group of founder cells at the periphery of the shoot apical meristem (SAM), a dome-shaped structure at the shoot apex that harbours a constant pool of stem cells throughout plant life (Barton, 2010). Concurrently, a low cell proliferation region, termed as the 'boundary zone' gets established at the interface that separates the primordium from the SAM (Hepworth and Lenhard, 2014; Wang et al., 2016). The basic form of the leaf consisting of the lamina and the petiole is established during primary morphogenesis, wherein leaf growth is primarily sustained by cell proliferation. The end of primary morphogenesis is marked by the switch from cell proliferation to differentiation and the formation of specific cell/ tissue types such as trichomes and stomata (Bar and Ori, 2014). Serrations are also initiated at this stage by outgrowth at specific sites along the base of the leaf margin. During secondary morphogenesis, differentiation of all the cell types is completed, and the leaf grows primarily by cell expansion (Bar and Ori, 2014; Du et al., 2018; Maugarny-Calès and Laufs, 2018).

The shape and size of the mature leaf can be regulated at each of the above three developmental stages by modulating the number of founder cells during initiation, or by regulating the rate, location and duration of cell proliferation and expansion (Gonzalez et al., 2012; Hepworth and Lenhard, 2014; Kalve et al., 2014). Besides, the timing of cell proliferation arrest, which directly affects the number of cells in mature leaves, is a major determinant of the final leaf size in a wide range of plant species (Gázquez and Beemster, 2017). In Arabidopsis leaves, arrest of cell proliferation occurs basipetally; cells towards the tip stop dividing and commit to differentiation (Donnelly et al., 1999; Andriankaja et al., 2012; Fox et al., 2018), while cells at the base continue to proliferate. Subsequently, the diffused boundary between the proliferation and differentiation regions remains at a constant distance from the base before being abruptly terminated (Andriankaja et al., 2012; Fox et al., 2018). Compensation also plays a key role in regulating leaf size, wherein a change in cell proliferation triggers an opposite effect on cell size at maturity, thus maintaining the mature leaf size relatively unaltered (Tsukaya, 2005; Hisanaga et al., 2015).

Genetic factors such as *GROWTH REGULATING FACTORS* (*GRFs*), *ANGUSTI- FOLIA3* (*AN3*) and the cytochrome P450-encoding gene *KLUH* (*KLU*) promote growth by maintaining the proliferative state of the cells in the proximal region (Horiguchi et al., 2005; Anastasiou et al., 2007; Kazama et al., 2010; Vercruyssen et al., 2014). The genetic modules that initiate the arrest of cell proliferation have also been described to a large extent in Arabidopsis (Gonzalez et al., 2012; Kalve et al., 2014; Du et al., 2018). Notably, two gene families that encode antagonistically acting transcription factors (TF) control the transition from cell proliferation to cell expansion: the *GROWTH REGULATING FACTORs* (*GRFs*) and the *CINCINNATA*-like *TEOSINTE BRANCHED 1*, *CYCLOIDEA*, *PROLIFERATING CELL FACTOR1/2* (*CIN-TCPs*) (Rodriguez et al., 2014; Sarvepalli and Nath, 2018). The spatiotemporal activities of *GRFs* are regulated by microRNA miR396. miR396 downregulates *GRF* transcripts in the distal region of the leaf, thereby restricting GRF activities towards the base (Rodriguez et al., 2010). GRFs interact with GRF-INTERACTING FACTOR 1/ANGUSTIFOLIA 3 (GIF1/AN3) and upregulate *CYCLIN B* (*CYCB*) expression to delay the proliferation-differentiation transition (Schneider et al., 2023). Eight *CIN-TCP* genes promote leaf maturation by triggering the transition of cell proliferation to differentiation in diverse eudicots including Arabidopsis (Sarvepalli and Nath, 2018). The spatiotemporal pattern of *CIN-TCP* transcripts are regulated by a combined action of their promoter activity and microRNA miR319 (Palatnik et al., 2003; Efroni et al., 2008). The miR319 activity prevents the accumulation of transcripts of five *CIN-TCPs* (*TCP2, 3, 4, 10, 24*), also known as *JAGGED AND WAVY TCPs* (*JAW-TCPs*), in the proximal region of the young leaf primordia (Palatnik et al., 2003; Nag et al., 2009). Expression of miR319-resistant form of *JAW-TCPs* with endogenous regulation leads to smaller leaves with fewer cells due to precocious proliferation arrest, while ectopic expression of miR319 results in large and wavy leaves due to a delay in the transition from proliferation to differentiation (Palatnik et al., 2003; Efroni et al., 2008; Challa et al., 2019). CIN-TCPs commit the leaf cells towards differentiation by modulating multiple pathways, such as auxin and cytokinin response, meristematic activity, and cell cycle progression (Sarvepalli and Nath, 2018).

The *CUP SHAPED COTYLEDON* (*CUC*) group of genes, which encode the NAM/ ATAF/ CUC (NAC) group of TFs, regulate boundary development in diverse angiosperms (Wang et al., 2016). The Arabidopsis *CUC* members *CUC1*, *CUC2*, and *CUC3* are consistently expressed in the boundary zones, and their absence leads to the fusion of adjacent organs such as cotyledons, sepals, stamens, and ovules (Aida et al., 1997; Ishida et al., 2000; Vroemen et

al., 2003). The *CUC* genes are also required for the maintenance of shoot meristem via the activation of the *SHOOT MERISTEMLESS* (*STM*) gene and its homologues (Aida et al., 1999; Hibara et al., 2006; Scofield et al., 2018). In leaf primordia, *CUC2* and *CUC3* are expressed at distinct foci along the margin, where they are necessary for the initiation and growth of serrations/ leaflets through a feedback mechanism involving auxin and the auxin efflux carrier PINFORMED1 (PIN1) (Nikovics et al., 2006; Bilsborough et al., 2011; Hasson et al., 2011; Maugarny-Calès et al., 2019). Interestingly, some of the gain-of-function phenotypes of *JAW-TCPs*, such as impaired SAM function, cotyledon fusion, and smooth leaf margin, are dependent on the downregulation of *CUC* activity (Koyama et al., 2007; Koyama et al., 2010; Koyama et al., 2017; Challa et al., 2019). While TCP3 inhibits *CUC1* and *CUC2* by activating the transcription of the miR164-encoding gene *MIR164A* to promote shoot morphogenesis (Koyama et al., 2007; Koyama et al., 2010), TCP4 protein interacts with CUC and inhibits their homo-dimerization and transactivation abilities to modulate serration formation and outgrowth (Rubio-Somoza et al., 2014).

Expression analysis of the miR319-encoding genes *MIR319A*, *MIR319B*, and *MIR319C* in Arabidopsis suggested their distinct developmental functions due to largely non-overlapping expression pattern (Nag et al., 2009). Whereas *MIR319A* and *MIR319B* promoter activity is not detected in leaves, *MIR319C* is strongly expressed in the leaf primordia (Nag et al., 2009; Shankar et al., 2023). However, the single loss-of-function mutants for miR319a and miR319b show a moderate decrease in leaf serration, and the *miR319a;miR319b* double mutant leaves lack serration, suggesting a role for *MIR319A* and *MIR319B* genes in leaf development (Koyama et al., 2017). However, the *miR319a;miR319b* leaves are as big as wild-type (Koyama et al., 2017), pointing towards a key role of miR319c in downregulating *JAW-TCP* activity during the early leaf growth. We had earlier demonstrated that JAW-TCPs transcriptionally repress the miR319-encoding gene *MIR319C* in the distal region to prevent miR319 accumulation, thereby establishing spatially separated proximal miR319 domain and distal JAW-TCP domain in incipient leaf primordia (Shankar et al., 2023). However, it is still unknown how the *MIR319* genes are transcriptionally activated in the early leaf primordia. Here, we demonstrate that CUC2 transcriptionally activates the *MIR319C* gene, and together with the products *MIR319A* and *MIR319B*, the mature miR319 sustains cell proliferation and promote leaf growth.

138 # Results

139

140 **A yeast one-hybrid screen identifies transcriptional activators of *MIR319C***

141

142 The *MIR319C* promoter activity is primarily detected at the shoot apex, more specifically at
143 the meristem-primordia boundary and in young leaf primordia (Shankar et al., 2023)
144 (**Figs. S1A, S1B**), suggesting that members of the transcriptome subset within this domain
145 activate *MIR319C* transcription. To identify such direct transcriptional regulators of *MIR319C*,
146 we screened a subset of yeast one-hybrid library containing 378 Arabidopsis transcription
147 factors enriched in the shoot apex for their ability to bind to the upstream regulatory region
148 (URR) of *MIR319C* (**Figs. S1C, S1D, Table S3**). Fifty seven TFs were identified that promoted
149 the growth of yeast cells when a 2736 bp URR was used as bait to drive the expression of the
150 *HISTIDINE3* (*HIS3*) selection gene (**Table S4**). Gene ontology analysis revealed that TFs
151 belonging to NAC, TCP, ETHYLENE RESPONSE FACTOR (ERF), BASIC LEUCINE
152 ZIPPER DOMAIN (bZIP), and BASIC HELIX LOOP HELIX (bHLH) families were over-
153 represented among the positive clones identified in the screen (**Fig. 1A**).

154

155 Interestingly, 5 out of the 6 NACs recovered from the Y1H screen (**Fig. S1E**) show comparable
156 DNA-binding preferences, the target DNA sequence being TT(G/A)CGT (Lindemose et al.,
157 2014), which is present at the 2619 nucleotide position upstream to the start of pre-*MIR319C*
158 sequence. The binding preference of these 5 NACs is also shared by other members of the
159 NAM, OsNAC7, NAC2, ANAC011, and AtNAC3 subgroup of the AtNAC TF family (Ooka
160 et al., 2003; Lindemose et al., 2014). To identify additional NAC members capable of binding
161 to the *MIR319C URR*, we chose 20 representative members from these 5 AtNAC subgroups
162 (**Fig S2A, S2B**) and tested in yeast for their binding ability to three non-overlapping *MIR319C*
163 *URR* fragments named as p^{distal} (-2736 to -1866 bp), p^{middle} (-1866 to -1106 bp), and $p^{proximal}$
164 (-1106 to -1 bp) (**Fig 1B**). Six NAC members including CUC1, CUC2 & CUC3 supported
165 yeast growth when p^{distal} was used as bait (**Fig 1C, Fig. S2B)**.

166

167 **CUC2 activates *MIR319C* in leaf primordia**

168

169 *CUC2*, the primary *CUC* member in leaves (Nikovics et al., 2006; Hasson et al., 2011), is active
170 throughout the shoot apex and initiating leaf primordia, overlapping the *MIR319C* domain
171 (**Fig S1A, S1B**). The overlapping expression pattern in early leaf primordia, and the ability of

172 CUCs to bind to *MIR319C* URR in yeast, led us to investigate if CUCs regulate *MIR319C*
173 promoter activity in leaves by determining *MIR319C* expression in mutants with altered *CUC2*
174 levels using a *GUS*-based reporter line for *MIR319C* promoter activity (*pMIR319C::GUS*$^{\#1}$)
175 (Nag et al., 2009; Shankar et al., 2023). We used an Image-J-based method to quantify the
176 domain of *pMIR319C::GUS* expression relative to the leaf length and termed it as relative GUS
177 domain (Shankar et al., 2023). The relative GUS domain was significantly reduced (median
178 ~0.35 compared to ~0.6 in Col-0) in *cuc2-1* leaves (Hasson et al., 2011) and was increased
179 (median ~0.75) in *cuc2-1D* (Larue et al., 2009), a line with elevated CUC2 activity (**Fig 1D,**
180 **1E**). The pre-*MIR319C* transcript level was ~1.5-fold lower and >2-fold higher in
181 *pMIR319C::GUS*$^{\#1}$;*cuc2-1* and *pMIR319C::GUS*$^{\#1}$*;cuc2-1D* seedlings, respectively (**Fig 1F**).
182 Together, these results suggest that CUC2 is required and sufficient to activate *MIR319C*
183 expression in leaf primordia.
184
185 ***CUC2* promotes cell proliferation in miR319-dependent manner in leaves**
186
187 Mature miR319 promotes cell proliferation by degrading the transcripts of five *JAW-TCP*s
188 (Palatnik et al., 2003; Efroni et al., 2008; Koyama et al., 2010; Challa et al., 2019). If CUC
189 proteins promote miR319 accumulation, inactivation of either *CUC2* or *MIR319C* is expected
190 to yield smaller leaves with fewer cells. To test this, we analysed the matures leaves of two
191 existing loss-of-function alleles of *CUC2*, *cuc2-1* and *cuc2-3* (Nikovics et al., 2006; Hasson et
192 al., 2011), and *miR319c-1*, a new allele of *MIR319* where the level of mature miR319c is
193 perhaps reduced (**Fig S4A, S4B**). None of these mutants showed any noticeable reduction in
194 mature leaf area or epidermal cell area (**Fig. 2A-C**, **Fig S3A, S3B**), perhaps because of the
195 hypomorphic nature of the mutant alleles and due to the presence of their redundant partners.
196 To test the genetic relationship between *CUC2* and *MIR319C*, we generated the double mutant
197 line *cuc2-3; miR319c-1* and analysed its leaf size parameters. The double mutant leaves were
198 nearly half the size of their respective parents (**Fig 2A, 2B, S3**), though the average area of
199 their pavement cells did not reduce (**Fig. 2C, 2D**). Thus, the *cuc2-3; miR319c-1* leaves were
200 made up of only ~2000 cells whereas the Col-0 leaves had ~4,500 cells (**Fig. 2E**), suggesting
201 reduced cell proliferation in the double mutant. The corresponding cell numbers for the
202 *cuc2-3* and *miR319c-1* leaves also reduced compared to the wildtype, but to a much less extent
203 (**Fig. 2E**). Fewer cells in *cuc2-3* and *miR319c-1* leaves is perhaps partly compensated by
204 slightly increased cell area (**Fig. 2D**), a phenomenon not observed in the *cuc2-3*; *miR319c-1*
205 double mutant leaves.

206

207 To determine the timing of this cell proliferation defect during leaf morphogenesis, we
208 performed confocal imaging of propidium iodide-stained primordia at 1, 3 and 5 days after
209 initiation (DAI) and analysed the images at the cellular level using morphographX tool. The
210 analysis revealed that while the cell areas of leaf primordia in all the genotypes at 1 DAI were
211 nearly homogenous, there was a distinct proximodistal gradient in cell growth at 3 and 5 DAI
212 marked by smaller cells at the base and larger cells in the distal region of the leaf primordia
213 (**Fig 3A**). There was a significant increase in average cell areas from 1-5 DAI in all the
214 genotypes, chiefly contributed by the larger cells in distal region of the primordia (**Figs 3A-C,**
215 **S3C**), an indication of onset of differentiation. Interestingly, the average cell area in
216 *cuc2-3;miR319c-1* leaf primordia (median~125μm^2) was significantly higher than Col-0,
217 *cuc2-3*, and *miR319c-1* genotypes at 3 DAI (median~100μm^2) (**Fig 3A, 3B**) but not at 1 DAI
218 (**Fig S3C**). The trend was also consistent at 5 DAI where *cuc2-3* and *cuc2-3;miR319c-1* had
219 higher average cell areas (median~150μm^2) compared to Col-0 and *miR319c-1*
220 (median~125μm^2) (**Fig 3C**). The cellular analysis further revealed that *cuc2-3;miR319c-1* had
221 a higher proportion of larger size cells (100-200μm^2 and >200μm^2) compared to wild type and
222 the parental genotypes at 3 DAI (**Fig S3D**), while *cuc2-3* and *cuc2-3;miR319c-1* mutants had
223 larger population of 200-500μm^2 and >500μm^2 cells and a corresponding lower proportion of
224 <250μm^2 cells at 5 DAI (**Fig S3E**). Cellular analysis suggested an altered cell growth pattern
225 in *cuc2-3;miR319c-1* leaf primordia marked by a precocious increase in pavement cell areas.
226 These results, together with those presented in **Fig. 1**, provides some genetic evidence that
227 CUC proteins promote cell proliferation in leaf primordia in a miR319c-dependent manner.
228

229 To investigate if *MIR319A* and *MIR319B* genes also regulate leaf size, we combined *cuc2-3*
230 and *miR319ab* (Koyama et al., 2017) and studied the leaf phenotypes in the higher-order
231 mutants. We observed a significant proportion of seedlings with narrow leaves, fused
232 cotyledons or arrested growth within the homozygous *cuc2-3;miR319a* and *cuc2-3;miR319b*
233 population (**Fig 4A**), which was not observed in either of the parent population. While 15.4%
234 each of seedlings within the *cuc2-3;miR319a* population exhibited narrow leaf and arrested
235 growth, 3.3% and 26% of the *cuc2-3;miR319b* seedlings had narrow leaves and arrested
236 growth/fused cotyledons, respectively (**Fig 4A**). We also observed a similar range of
237 phenotypes in the *cuc2-3;miR319a/+;miR319b/+* and *cuc2-3;miR319a/+;miR319b* mutant
238 population (**Fig 4A**). For simplicity, we shall denote *cuc2-3;miR319a/+;miR319b/+* and

239 *cuc2-3;miR319a/+;miR319b* mutants as *cuc2-3;miR319ab* from hereon. Next, we measured
240 the leaf areas, pavement cell area and number in matured first pair of leaves from the seedlings
241 having narrow leaves within the *cuc2-3;miR319a*, *cuc2-3;miR319b*, and *cuc2-3;miR319ab*
242 population. The leaf areas of *cuc2-3;miR319a* and *cuc2-3;miR319b* mutants were significantly
243 lower (2 to 3-fold) than the wild-type and the parent genotypes (**Fig 4B, 4C**). The leaf areas in
244 *cuc2-3;miR319ab* were reduced to the same extent of *cuc2-3;miR319a* and *cuc2-3;miR319b*
245 double mutants (**Fig 4B, 4C**). Interestingly, the lower leaf areas in *cuc2-3;miR319ab* mutants
246 was due to the reduction in both pavement cell areas and cell numbers (**Figs 4D, S5A, S5B**).
247 While the pavement cell shapes of *cuc2-3;miR319a/+;miR319b/+* mutant was similar to the
248 wild-type, *cuc2-3;miR319a/+;miR319b* had less lobed and more elongated cells (**Fig S5B**),
249 indicating an alteration in cell growth pattern.
250
251 We speculated that low miR319 levels in the *cuc2-3;miR319a* and *cuc2-3;miR319b* mutants in
252 would cause an increase in *JAW-TCP* activity during embryogenesis, resulting in cotyledon
253 fusion and seedling arrest phenotypes. To test this possibility, we established *cuc2-1;GR*$^{\#2}$ by
254 crossing *cuc2-1* mutant to Col-0;*GR*$^{\#2}$ (Shankar et al., 2023), a line where miR319-resistant
255 dexamethasone (DEX) inducible form of TCP4 protein is expressed under its endogenous
256 promoter in the wild-type background. 12/583 (2%) seedlings obtained from the seeds of the
257 DEX-treated *cuc2-1;GR*$^{\#2}$ flowering plants (**See *Methods***) exhibited cotyledon separation
258 defects while all the seedlings from the ethanol-treated Col-0;*GR*$^{\#2}$ and *cuc2-1;GR*$^{\#2}$ plants or
259 the DEX-treated Col-0;*GR*$^{\#2}$ had well-separated cotyledons (**Fig S4C**). The above results
260 suggest that the *CUC2*-mediated activation of miR319c also contributes to the downregulation
261 of *JAW-TCP* activity during the establishment of the SAM-cotyledon boundary.
262
263 To further explore the functional redundancy among the three *MIR319* genes in leaf cell
264 proliferation, we determined the final leaf area, pavement cell area and number in the first pair
265 of leaves in the triple mutants obtained by combining *miR319ab* and *miR319c-1* genotypes.
266 The higher order *miR319abc* mutants, i.e., *miR319a;miR319b;miR319c-1/+*,
267 *miR319a;miR319b/+;miR319c-1*, and *miR319a;miR319b;miR319c-1* had highly reduced leaf
268 areas (median 5-8 mm^2) compared to the wild-type (median~22 mm^2) (**Fig 5A, 5B**). The
269 reduction in leaf areas was only due to significantly lower cell numbers (~4-fold reduction)
270 (**Fig 4D**) but not cell areas (**Fig S5A, S5B**). Together, the above results suggests functional
271 redundancy among three *MIR319* genes and a critical role for *CUC2-MIR319* pathway in
272 promoting leaf size via cell proliferation in leaf primordia.

273 **CUC2 binds and activates *MIR319C* transcription**

274

275 We earlier showed that CUCs specifically bind to the distal URR of *MIR319C* containing the
276 putative CUC binding site in yeast (**Fig 1E**). To study the importance of the CUC binding site
277 for *MIR319C* promoter activity, we generated a *GUS*-based reporter line for *MIR319C*
278 promoter carrying mutations in the CUC binding site (*mCUCBSpMIR319C::GUS*) (**Fig 5C**)
279 and determined the relative GUS domain in the *mCUCBSpMIR319C::GUS* expressing leaf
280 primordia. The relative GUS domain was significantly reduced in the leaf primordia expressing
281 *mCUCBSpMIR319C::GUS* transgene as compared to the wild-type *pMIR319C::GUS*$^{\#2}$
282 (Shankar et al., 2023) expressing leaf primordia (**Fig 5D-F**), suggesting that the CUC binding
283 site is required for the *MIR319C* promoter activity.

284

285 Next, to determine if CUC2 directly activates *MIR319C* transcription, we induced CUC2
286 activity in 10-day-old *pRPS5A::CUC2-GR-HA* seedlings (Tian et al., 2014) by treating them
287 with dexamethasone (DEX) for two hours in the presence of the protein synthesis inhibitor
288 cycloheximide (CHX) and measured pre-*MIR319C* levels by RT-qPCR. CUC2 was able to
289 significantly elevate pre-*MIR319C* transcript levels (~2-fold), similar to transcripts of its
290 known direct target *CUC3*, both in the presence and the absence of CHX (**Fig 5G**), suggesting
291 that *MIR319C* could be a direct target of CUC2. The above results indicate that CUC2 binds
292 and activates *MIR319C* transcription in early leaf primordia.

293

294 ***CUC-MIR319C-JAW-TCP* module regulates leaf size**

295

296 The gain-of-function line for *CUC2* activity, *cuc2-1D,* has larger than wild-type leaf areas due
297 to increased cell numbers (Larue et al., 2009). Since *MIR319C* expression was elevated in
298 *cuc2-1D* (**Fig 1D-F**), we investigated if the increased leaf size in *cuc2-1D* is due to reduced
299 *JAW-TCP* activities. We crossed the *TCP4* overexpression line Col-0;*GR*$^{\#1}$ (Challa et al., 2016)
300 to *cuc2-1D* and studied leaf areas in ethanol and DEX-treated F1 progeny. Although
301 Col-0;*GR*$^{\#1}$ line contains a DEX-inducible miR319-resistant TCP4, it resembles wild-type
302 under non-inductive conditions (**Fig 6A**), as reported earlier (Challa et al., 2016). The average
303 first leaf areas of ethanol-treated Col-0;*GR*$^{\#1}$x *cuc2-1D* F1 individuals were significantly higher
304 (median~32 mm^2) than ethanol-treated Col-0;*GR*$^{\#1}$x Col-0 F1 control (median~23 mm^2)
305 (**Fig 6A, 6B**). Induction of *rTCP4* activity in both Col-0;*GR*$^{\#1}$x Col-0 F1 and Col-0;*GR*$^{\#1}$x
306 *cuc2-1D* F1 seedlings resulted in the formation of smaller leaves with similar areas (median~14

307 mm^2) (**Fig 6A, 6B**), suggesting that *CUC2* promotes leaf size via miR319-mediated
308 downregulation of *JAW-TCPs*.
309
310 Overexpression of miR319 leads to the formation of larger than wild-type leaves with deeper
311 serrations (**Fig 6C**) (Efroni et al. 2008; Challa et al. 2019). The lack of *CUC2* activity in the
312 miR319 overexpression background only affected the serration formation but did not alter the
313 leaf area (**Fig 6C, 6D**). The similar leaf areas of *pBLS>>miR319a* and
314 *cuc2-1;pBLS>>miR319a* mutants strongly suggests that the *MIR319-JAW-TCP* module
315 regulates leaf size downstream of *CUC2*. These results also demonstrate that the
316 *CUC-MIR319-JAW-TCP* module regulates leaf size and serration pattern by distinct
317 mechanisms.
318
319 ***CUC2* and *JAW-TCP* activities establish *MIR319C* expression domain in early leaf**
320 **primordia**
321
322 We previously demonstrated that JAW-TCPs downregulate *MIR319C* expression in the distal
323 region of the leaf primordia (Shankar et al., 2023). A previous study showed that *JAW-TCPs*
324 transcriptionally inhibit the expression of *CUCs* during early shoot organogenesis (Koyama et
325 al., 2007). To investigate if *JAW-TCPs* transcriptionally downregulate *CUC2* and thereby
326 *MIR319C* expression in leaf primordia, we studied the domain of expression of the promoter-
327 reporter line for *CUC2*, i.e., *pCUC2::GUS* (Nikovics et al., 2006) in knockdown line for all
328 five *JAW-TCPs*, i.e., *jaw-D* (Palatnik et al., 2003). The expression pattern of *CUC2* was highly
329 similar in Col-0 and *jaw-D* leaf primordia (**Fig 7A**). To support the observation that *JAW-TCPs*
330 do not transcriptionally downregulate *CUC2* expression during early stages of leaf primordia,
331 we studied the domain of *pCUC2::GUS* expression in seedlings heterozygous for Col-0;*GR*$^{\#1}$
332 transgene, i.e., Col-0 x Col-0;*GR*$^{\#1}$ F1. The expression pattern of *pCUC2::GUS* did not vary
333 significantly between ethanol and DEX-treated early Col-0 x Col-0;*GR*$^{\#1}$ F1 leaf primordia
334 (**Fig S5C**), suggesting *JAW-TCPs* do not affect *CUC2* transcription in early leaf primordia.
335 JAW-TCPs also suppress *CUC2* and *CUC3* activities at the post-transcriptional level via
336 miR164a upregulation (Koyama et al., 2010) and at the protein level through physical
337 interaction (Rubio-Somoza et al., 2014). Hence, to test if JAW-TCPs downregulate *MIR319C*
338 expression at least partly by modulating *CUC2* activity, we studied *MIR319C* promoter activity
339 in mutants with altered *CUC2* and *JAW-TCP* levels.
340

First, we looked at the *MIR319C* expression domain in Col-0;*GR*$^{\#2}$ (Shankar et al., 2023) and *cuc2-1D;GR*$^{\#2}$ leaf primordia where *rTCP4* activity can be induced by DEX treatment in wild-type and *cuc2-1D* genetic backgrounds, respectively. Under mock conditions, the *pMIR319C::GUS* domain was distally expanded in *cuc2-1D;GR*$^{\#2}$ leaf primordia compared to Col-0;*GR*$^{\#2}$ control (median~0.55 in *cuc2-1D;GR*$^{\#2}$ mock compared to ~0.4 in Col-0;*GR*$^{\#2}$ mock) (**Fig 7B, 7C**). While *rTCP4* induction greatly restricted the *MIR319C* expression proximally in the Col-0 background (median~0.25), the *pMIR319C::GUS* domain was only restricted to near wild-type level (median~0.35) when *rTCP4* activity was induced in the *cuc2-1D* background (**Fig 7B, 7C**), indicating that *MIR319C* expression domain is established by *CUC2* and *JAW-TCPs* via independent pathways.

We also looked at *MIR319C* expression domain in mutants where *miR319a* is overexpressed in *cuc2-1* and *cuc2-1D* mutant backgrounds. Similar to earlier results in (**Fig 1D, 1E**), the loss of *CUC2* activity (*cuc2-1*) alone reduced the domain of *MIR319C* expression (median~0.3) compared to wild-type (median~0.45) (**Fig 7D, 7E**). In contrast, the downregulation of all the *JAW-TCPs* (*pBLS>>miR319a*) or elevation of *CUC2* activity (*cuc2-1D*) resulted in the distal expansion of the *MIR319C* expression domain (median~0.5) (**Fig 7D, 7E**). The *MIR319C* expression domain in *cuc2-1;pBLS>>miR319a* leaf primordia (median~0.4) was similar to that of the wild-type. In addition, *cuc2-1D;pBLS>>miR319a* leaf primordia did not show a further increase in *MIR319C* expression domain compared to either of its parent genotypes (**Fig 7D, 7E**). These results support the earlier conclusion that *CUC2* and *JAW-TCPs* independently regulate the *MIR319C* expression domain in early leaf primordia.

Discussion

The miR319-CIN-TCP module regulates leaf morphology in diverse eudicots by affecting the timing of pavement cell proliferation to differentiation transition (Palatnik et al., 2003; Efroni et al., 2008; Shleizer-Burko et al., 2011; Challa et al., 2019). Although the molecular mechanisms for miR319-CIN-TCP mediated regulation of leaf morphology had been described (Sarvepalli and Nath, 2018; Challa et al., 2019; Challa and Rath et al., 2021), the genetic basis for the transcriptional activation of *MIR319* and *CIN-TCP* genes during leaf growth was unknown. In this study, we provide evidence to suggest that CUCs bind to the *MIR319C* promoter and activate transcription in leaf primordia. All three CUCs specifically bound to the

374 *MIR319C* distal promoter fragment that harboured a unique CUC binding site, TTACGT, in
375 yeast (**Fig 1C**). Mutations in the CUC binding site resulted in more proximal restriction of
376 *MIR319C* expression domain (**Fig 5D-F**), a phenotype that was also observed in the *cuc2-1*
377 mutant (**Fig 1D, 1E**). While *cuc2-1* had lower pre-*MIR319C* levels, transient induction of
378 CUC2 activity in presence of protein synthesis inhibitor was sufficient to increase the cellular
379 pre-*MIR319C* transcript levels (**Fig 1F, 5G**), suggesting CUC2 activity is both required and
380 sufficient to promote *MIR319C* transcription. However, it remains to be clarified whether
381 CUC2 directly binds to the cis element on the *MIR319C* promoter in planta and if CUC2
382 requires additional factors to activate *MIR319C* expression. Nevertheless, the evidence from
383 this study suggests a model where ubiquitous *CUC2* expression in the initiating leaf primordia
384 activates *MIR319C* transcription which results in high miR319c activity, whereas during later
385 stages of primordia growth, *CUC2* expression and hence miR319c activity gets restricted
386 towards the SAM-leaf boundary and proximal leaf margins (**Fig S6**).
387
388 **What is the significance of *CUC2*-mediated activation of *MIR319C* in leaf primordia?**
389
390 In developing leaves, miR319-directed cleavage of *JAW-TCP* transcripts is required for proper
391 timing of the transition between cell division and differentiation (Palatnik et al., 2003; Efroni
392 et al., 2008; Challa et al., 2019). Interestingly, loss of *CUC2* barely affects cell proliferation in
393 leaves, suggested by a small yet consistent decrease in leaf size chiefly due to reduced cell
394 number (**Figs 2, 4, S3A, S3B**). The negative effect of *CUC2* loss on leaf cell proliferation is
395 likely due to reduced miR319c levels as a result of partial downregulation of *MIR319C*
396 promoter activity (**Fig 1D, 1E**). The role of CUC2-mediated activation of *MIR319C* in leaf cell
397 proliferation was further revealed by the strong reduction in cell numbers in mature leaves of
398 the *cuc2-3;miR319c-1* double mutant (**Fig 2**). *miR319c-1* has a T-DNA insertion 528 bp
399 upstream of the pre-*MIR319C* transcript (**Fig S4A**). *GUS*-based *MIR319C* promoter deletion
400 reporter line carrying only 533 bp showed reduced promoter activity as compared to 1866 bp
401 and full length (2736 bp) promoter lines (**Fig S4B**). Thus, the presence of 4.7 kb T-DNA in the
402 *MIR319C* promoter is likely to negatively impact the transactivation ability of TFs (including
403 *CUC2*) that bind to distal region, leading to reduced miR319c levels. We speculate that
404 *cuc2-3;miR319c-1* mutant has lower levels of miR319c than the individual parent genotypes
405 due to additive loss of *CUC2* and other TF-mediated activation of *MIR319C* transcription. The
406 cellular analysis during early stages of *cuc2-3;miR319c-1* leaf primordia growth revealed an
407 increased proportion of enlarged cells as early as 3 DAI, which persisted even at 5 DAI

408 (**Fig 3**). These observations suggest a scenario where reduced miR319c levels leads to a
409 precocious transition of pavement cells from proliferation into differentiation due to elevated
410 JAW-TCP activity, particularly at the base of the leaf primordia. The hypothesis is further
411 supported by epistatic interaction observed between *CUC2* and *JAW-TCPs*, where miR319
412 overexpression led to increased leaf size even in *cuc2-1* background and ectopic *JAW-TCP*
413 activity resulted in smaller than wild-type leaves in *CUC2* overexpression and wild-type
414 backgrounds (**Fig 6**). In sum, we demonstrate *CUC2* as an activator of *MIR319C* expression in
415 leaf primordia and propose a novel function for *CUC2* in promoting pavement cell division
416 during early stages of leaf growth via *MIR319C* activation. Using Y1H approach, we
417 uncovered other potential activators of *MIR319C* transcription such as members of YABBY,
418 LBD, and WOX TF families (**S4 Table**), which show highly overlapping expression patterns
419 with *MIR319C* and are known to have roles in leaf growth (Wu et al., 2008; Sarojam et al.,
420 2010; Nakata et al., 2012). It will be an interesting future prospect to investigate whether these
421 TFs directly associate with *MIR319C* promoter and activate its expression in planta.
422
423 **Role of *CUC2-MIR319-JAW-TCP* module in pavement cell division and growth**
424
425 *miR319a;miR319b* and *miR319c-1* mutants had wild-type leaf areas whereas the *miR319abc*
426 triple mutants displayed smaller leaves with fewer cells of unchanged areas (**Figs 5A, 5B, 4D,**
427 **S5A, and S5B**). The leaf and cell phenotypes of *miR319abc* were similar to *rTCP4*
428 overexpression lines, supporting the conclusion from earlier kinematic studies that *miR319-*
429 *JAW-TCP* module regulates pavement cell proliferation to differentiation transition, but has
430 little effect on post-mitotic cell expansion (Challa et al., 2019). Together the above
431 observations strongly suggest a functional redundancy among *MIR319* genes in suppressing
432 JAW-TCP activity at the base of the primordia. While *miR319b* mutant completely lacks
433 miR319b activity (Koyama et al., 2017), both *miR319a* and *miR319c-1* lines are likely to retain
434 low levels of miR319a and miR319c activities, respectively (Nag et al., 2009; Koyama et al.,
435 2017) (**Fig S4A, S4B**). We used knockdown alleles of *miR319a* and *miR319c* to study genetic
436 interaction with *CUC2* and among *MIR319* genes as *miR319* knockouts are expected to have
437 high levels of ectopic *JAW-TCP* activity which may lead to embryo lethality and/or seedling
438 arrest (Palatnik et al., 2003; Koyama et al., 2017). The F2 population from the cross between
439 *cuc2-3/cuc2-1* and *miR319ab* exhibited a range of phenotypes that included narrow leaves and
440 fused cotyledons (**Fig S3A, S3F**), suggesting a role for *CUC2-MIR319* pathway in leaf growth
441 and cotyledon separation. To our surprise, even the homozygous *cuc2-3;miR319a* and

442 *cuc2-3;miR319b* population and the *cuc2-3;miR319ab* triple mutants displayed similar range
443 of leaf and cotyledon defects (**Fig 4**), probably due to penetrance in miR319 activity. The roles
444 of the *CUC2-MIR319* module in SAM establishment and cotyledon separation have been
445 demonstrated earlier (Koyama et al., 2007; Koyama et al., 2010; Koyama et al., 2017), but its
446 role in pavement cell proliferation has not been explored. Interestingly, unlike the
447 *miR319abc* mutants which had fewer cells of wild-type areas, the *cuc2-3;miR319ab* leaves had
448 lower cell numbers and cell areas (**Fig S5**). What could be the underlying cause for the
449 difference in cell growth pattern between *miR319abc* and *cuc2-3;miR319ab* mutants? Previous
450 studies have demonstrated that severe defects in leaf cell proliferation often induces post-
451 mitotic cell expansion leading to larger than wild-type cells. This phenomenon of coordinated
452 cell growth during leaf development is termed as compensation (Tsukaya, 2005). Recent
453 genetic and kinematic studies suggests that compensation is not a passive result of low cell
454 proliferation but rather a genetically regulated active mechanism (Hisanaga et al., 2015;
455 Tsukaya, 2019). Moreover, compensation is highly dependent on the extent of changes in
456 causal gene activity and can involve both cell autonomous and non-autonomous mechanisms
457 (Hisanaga et al., 2015; Vercruysse et al., 2021). We speculate that *CUC2* may promote
458 compensation in leaves independent of *MIR319C* activation. Thus, the lack of *CUC2* and
459 *MIR319A/B* activities would lead to premature proliferation arrest due to ectopic *JAW-TCP*
460 activity and impaired compensation via an unknown genetic pathway, resulting in leaves with
461 reduced cell numbers and areas. Previous studies have demonstrated that JAW-TCPs repress
462 the activities of all three *CUCs* at the mRNA and protein levels (Koyama et al., 2010; Rubio-
463 Somoza et al., 2014). Hence, ectopic *JAW-TCP* activity would feedback to further
464 downregulation of *CUC* activity and accentuate the cell proliferation and expansion defects in
465 *cuc2-3;miR319ab* mutants during leaf growth.
466
467 **How is the *MIR319C* expression domain established and maintained in leaf primordia?**
468
469 Here, we demonstrate that CUC2 activates *MIR319C* expression throughout the initiating leaf
470 primordia and at the base during later stages of leaf growth. We previously showed that JAW-
471 TCPs bind to *MIR319C* and repress its transcription in the distal region of the early leaf
472 primordia (Shankar et al., 2023). Interestingly, *CUC2* is initially expressed throughout the
473 primordia but restricted towards the base around the 150 μm stage coinciding with the onset of
474 distal *TCP4* expression (**Fig 7**). This raised a possibility that these two processes are linked and

475 lead to the restriction of *MIR319C* expression. However, we show that JAW-TCPs repress
476 *MIR319C* expression independent of *CUC2* activity (**Fig 7**), suggesting that *CUC2*-mediated
477 activation and *JAW-TCP*-mediated repression establish the basal *MIR319C* expression domain
478 via independent mechanisms. Although *MIR319C* expression highly coincided with the cell
479 proliferation zone, we previously demonstrated that *MIR319C* expression domain remained
480 unchanged in mutants with altered cell proliferation pattern (Shankar et al., 2023). This
481 evidence suggests that changes in the proliferation status of cells may not feedback to regulate
482 *MIR319C* expression. Previous modelling-based studies on leaf morphogenesis suggest that
483 cell growth induced mechanical forces could feedback and regulate growth and gene
484 expression (Kuchen et al., 2012; Fox et al., 2018). It will be interesting to investigate if such
485 feedback mechanisms play role in maintenance of basal *MIR319C* expression domain.
486 Additionally, some of the outstanding questions regarding the establishment of *MIR319C*
487 expression domain are as follows: Which genetic factors specifically promote *JAW-TCP*
488 expression in the distal region of the 150 μm primordia? How is *CUC2* expression, which is
489 ubiquitous during leaf initiation, later restricted towards the SAM-leaf boundary and proximal
490 margins of the leaf primordia? Answers to these questions will advance our understanding of
491 the molecular mechanisms that divide the uniformly proliferating primordia into two
492 contrasting domains of cell proliferation and differentiation and subsequently coordinate
493 growth across these zones during leaf morphogenesis.
494
495 Together, our data is consistent with a model where *CUC2* upregulates *MIR319C* expression
496 to maintain high miR319c levels, which together with miR319a and miR319b, restricts JAW-
497 TCP activity towards the distal region of the growing leaf primordia. High JAW-TCP protein
498 levels due to transcriptional activation leads to repression of *MIR319C* promoter activity in the
499 distal region (Shankar et al., 2023). CUC2-mediated activation of *MIR319C* and the miR319-
500 JAW-TCP feedback loop contributes to the establishment of spatially separated growth
501 domains of basal cell proliferation and distal cell differentiation in leaf primordia (**Fig S6**). We
502 propose that the *CUC2-MIR319-JAW-TCP* module is critical for spatiotemporal patterning of
503 cell proliferation in Arabidopsis leaf primordia. As the *CUC*, *MIR319*, and *JAW-TCP* genes
504 are conserved across plant evolution, it will be worthwhile to investigate if *CUC2-MIR319-*
505 *JAW-TCP* module regulates leaf growth in other plant species, especially those that exhibit
506 basipetal mode of growth.
507

508 **Context-dependent effect of *CUC2* on cell proliferation during organ morphogenesis**
509
510 During embryogenesis, all three *CUCs* are expressed at the junction between the SAM and the
511 cotyledons, where they redundantly repress cell proliferation to establish a boundary zone and
512 allow for the separation and subsequent outgrowth of the cotyledons (Vroemen et al., 2003;
513 Hibara et al., 2006; Scofield et al., 2018). Later on during leaf morphogenesis, CUC2 protein
514 accumulates at certain foci (termed sinus) along the leaf margin and induces serration
515 formation by inhibiting cell proliferation locally at the sinus region (Nikovics et al., 2006;
516 Bilsborough et al., 2011; Hasson et al., 2011). In addition, CUC2 promotes serration outgrowth
517 (termed tooth) via a non-cell autonomous mechanism involving *CUC3*, cytochrome P450
518 protein encoding *KLUH/CYP78A5*, and auxin response (Maugarny-Calès et al., 2019). These
519 studies point towards a dual role for CUC2 during serration formation and outgrowth where it
520 initially represses cell proliferation at the sinus region but promotes cell proliferation-induced
521 tooth outgrowth during later stages. Interestingly, expression of *miR164*-resistent *CUC2* in the
522 boundary zone during flower development led to a significant enlargement of boundaries
523 between sepal primordia due to increased cell proliferation (Laufs et al., 2004; Sieber et al.,
524 2007). Here, we show that *CUC2* promotes and maintains pavement cell proliferation via the
525 miR319-JAW-TCP pathway in early leaf primordia. Our data supports the notion that *CUC2*
526 can either activate or repress cell proliferation depending on the developmental stage and the
527 type of tissue it is expressed and regulate organ morphology. So far, only a few direct
528 downstream targets of CUCs have been identified (Takeda et al., 2011; Li et al., 2020; Aida et
529 al., 2020). By integrating spatial transcriptomics, whole-genome binding, and proteomics
530 experiments, future research could unveil the molecular mechanisms by which CUC2 exerts
531 context-dependent activation and repression.
532
533 **Do *CUCs* act as growth polarity organisers during leaf morphogenesis?**
534
535 Evidence from previous kinematics, genetics and modelling-based studies suggest that
536 morphogenesis of a simple cone-like primordium to complex planar mature leaf involves
537 highly coordinated spatiotemporal regulation of key parameters such as cell growth and
538 division rates, growth orientation and tissue deformation (Kuchen et al., 2012; Fox et al., 2018;
539 Sarvepalli et al., 2019). Growth polarity is apparent in early primordia where the proximal
540 region grows at a faster rate due to high cell proliferation, whereas distal region displays lower
541 growth rates and transitions into differentiation (Kuchen et al., 2012; Fox et al., 2018). Previous

542 studies proposed *CUC* as a growth polarity organizer, which, according to growth prediction
543 models is a factor that is highly expressed at the base and drives differential growth by
544 upregulating factors that promote growth and proliferation (Kuchen et al., 2012; Sarvepalli et
545 al., 2019). As mentioned earlier, CUCs are highly expressed at the boundaries and can regulate
546 growth at leaf margin by modulating auxin transport, activating factors that either promote or
547 repress cell proliferation (Bilsborough et al., 2011; Maugarny-Calès et al., 2019). It remains to
548 be seen if CUC-mediated promotion of pavement cell proliferation also involves some of these
549 mechanisms that exist in the context of serration outgrowth. Here, we demonstrate a novel role
550 of CUC2 in upregulating miR319c levels that results in low proximal JAW-TCP activity in
551 leaf primordia. JAW-TCPs are known to inhibit cell proliferation factors including GROWTH
552 REGULATION FACTOR (GRF) and GRF- INTERACTING FACTOR (GIF) which promote
553 growth and proliferation via activation of several cell cycle genes, including *CYCLINB1;1*
554 (Horiguchi et al., 2005; Schneider et al., 2024). Overall, CUC2-mediated activation of
555 *MIR319C* would enhance growth and proliferation in the proximal region, thus providing proof
556 for the role of *CUCs* as growth polarity organizer during leaf morphogenesis. In animal models,
557 it has been well established that boundaries function as morphogen providers to pattern organ
558 growth during embryogenesis (Meinhardt, 2009; Kicheva and Briscoe, 2023). The role of
559 CUC2 as a growth polarity organizer also raises an interesting possibility that boundaries can
560 serve as growth organizers during organ morphogenesis in plants. Future research could
561 explore mechanisms that link boundary gene networks with growth regulatory modules to test
562 this possibility.
563

564 ## Materials and Methods

565

566 **In silico screening for SAM and leaf primordia-specific transcription factors**

567 To identify SAM and leaf primordia-specific TFs, we took advantage of studies that generated
568 cellular-resolution maps of genes whose mRNA is actively translated in different domains
569 within the SAM and leaf primordia (Tian et al., 2014; 2019). We considered genes that are
570 active in the *CLV3*, *WUS*, *UFO* expression domains of the SAM, *LAS* expression domain of
571 the SAM-leaf boundary, and the *AS1* expression domain of the leaf primordia. We overlapped
572 the 4426 SAM and leaf primordia-specific genes with the list of 1956 genome-wide
573 Arabidopsis TFs (Pruneda-Paz et al., 2014) and obtained 343 TFs expressed explicitly in the
574 SAM and leaf primordia domains **S1 Table**. We also scanned the 2.7 kb URR of *MIR319C* for

575 TF binding sites using the publicly available transcription factor binding site (TFBS) prediction
576 tool (PlantPAN 3.0 - *http://plantpan.itps.ncku.edu.tw*). We recovered several potential DNA-
577 binding motifs on the *MIR319C* promoter, including TCP, KNOX, YABBY, NAC and HD-
578 like TF-binding consensus. We listed 49 representatives from the top 5 TF families recovered
579 from the TFBS prediction software **S2 Table**. Next, we combined this list with the previously
580 obtained 343 SAM and leaf primordia-specific TFs to get a final list of 378 TF candidates for
581 the yeast one-hybrid screen **S3 Table**.
582
583 **Yeast transformation**
584 Yeasts were transformed with the desired DNA constructs (plasmids) by the high-efficiency
585 LiAc-PEG method described by Walhout and Vidal, 2001, with minor modifications. A single
586 colony of host strain was inoculated in 10 ml YPAD (Bacto yeast extract-1g, Tryptone-1g,
587 Dextrose-2g, and Adenine sulphate-10mg per 100ml) and incubated overnight at 30ºC with
588 constant shaking. The next day, the suitable culture volume was inoculated into 200 ml of fresh
589 YPAD solution to an initial OD of 0.2 and kept at 30ºC with constant shaking until an OD of
590 0.6-0.8 was reached. Cells were pelleted down at 700 g for 10 min and washed twice with 5 ml
591 of sterile water. The cells were washed with 2.5 ml of LiAc-TE (0.1 M LiAc, Tris- 10 mM,
592 EDTA- 1mM) solution. Cells were finally resuspended in 2 ml of LiAc-TE solution. A mixture
593 containing 280 µL of 50% PEG (Mol wt 3350, Sigma-Aldrich, USA), 36 µL of 1 M LiAc in
594 TE, 6 µL of 10 mg/ml boiled carrier DNA (D-3159, Sigma-Aldrich, USA) was prepared and
595 added to 1.5 ml microfuge tubes containing 60 µL cells and 100 ng of DNA construct. The cell
596 suspension was vortexed briefly and incubated at 30ºC with constant shaking for 30 min. Cells
597 were transferred into a water bath maintained at 42ºC for 30 min. Cells were pelleted, washed
598 twice with sterile water, resuspended in 100 µL sterile water, and plated onto appropriate
599 media.

600 For the Y1H screen, transformations were carried out in 96 well-format described by Walhout
601 and Vidal, 2001. Yeast cells were prepared as described in the high-efficiency protocol. 20 µL
602 of cell suspension (containing LiAc-PEG-carrier DNA) were transferred to each well of a
603 sterile U-bottom 96-well plate (3795, Corning, USA). 100 ng of plasmid and 100 µL of
604 TE/LiAc/PEG solution (50% PEG and 0.1 M LiAc in TE) were individually added and
605 resuspended carefully using a multichannel pipette. 96-well plate was incubated at 30ºC with
606 constant shaking for 30 min. Cells were transferred to a water bath maintained at 42ºC for 30
607 min. Cells were pelleted at 700 g for 5 min. To each well, 120 µL of sterile water was added,

608 and 100 µL was removed directly to get rid of PEG in the supernatant. Finally, cells were
609 resuspended in the remaining 20 µL water and spotted on appropriate media.

610 **Yeast bait, prey, and diploid generation**

611 The full length (2.7 kb) and the non-overlapping promoter fragments, i.e., -2694-1866 (p^{distal}),
612 -1866-1107 (p^{middle}), and -1107+35 ($p^{proximal}$) of *MIR319C* were amplified from *pMIR319C-*
613 *P4P1R* entry clone using Taq DNA polymerase and cloned into pENTR/D-TOPO vector
614 (K240020, Invitrogen, USA) according to the manufacturer's instructions. The entry clones
615 were confirmed by Sanger sequencing before cloning upstream to the *minimalPro::HIS3*
616 cassette of *pMW#2* (Gift from Ram Yadav, IISER Mohali, INDIA) by LR reaction. Y1H baits
617 were generated according to the protocol described by Fuxman Bass et al., 2016. Briefly, the
618 *pMIR319C* containing *pMW#2* reporter constructs were linearized with *Xho*I (R0146, New
619 England Biolabs, USA) and integrated into the mutant *HIS3* locus of the *YM4271* host strain
620 (Gift from Ram Yadav, IISER Mohali, INDIA) using the high-efficiency LiAc-PEG
621 transformation method described by Walhout and Vidal, 2001. Following transformation, yeast
622 cells were plated on the synthetic complete media lacking histidine (Sc-His) media (Walhout
623 and Vidal, 2001) and incubated at 30ºC till colonies appeared. Post growth, genomic DNA was
624 extracted individually from 3-4 colonies, and the integration of the *MIR319C* promoter
625 fragment was confirmed by PCR. All primer sequences used for cloning are mentioned in **S5**
626 **Table**.

627 To generate the prey strains for the Y1H screen, each of the 384 TF-encoding plasmids was
628 individually purified from corresponding glycerol stocks of the 1956 DEST-U Arabidopsis TF
629 ORFeome collection (CD4-89, ABRC, USA) using QIAprep Spin Miniprep Kit. 100 ng of
630 purified plasmid were individually transformed into Yalpha1867 strain (Gift from Dr. Ram
631 Yadav, IISER Mohali, INDIA) using the high throughput 96-well format transformations
632 protocol described earlier. Following transformation, the cells were spotted on synthetic
633 complete media lacking tryptophan (Sc-Trp) media and incubated at 30ºC till colonies
634 appeared.
635
636 To generate the diploids used in the Y1H assay, prey TF-encoding plasmids was individually
637 purified from corresponding glycerol stocks of the 1956 DEST-U Arabidopsis TF ORFeome
638 collection (CD4-89, ABRC, USA) using QIAprep Spin Miniprep Kit. 100 ng of purified
639 plasmid were individually transformed into *pMIR319C* baits using the high-efficiency LiAc-

640 PEG method described earlier. Following transformation, the cells were spotted on synthetic
641 complete media lacking histidine and tryptophan (Sc-His-Trp) media and incubated at 30ºC till
642 colonies appeared.
643
644 **Yeast one-hybrid (Y1H) screen/ assay**
645 The auto activity of yeast baits on Sc-His due to minimal *HIS3* expression was determined
646 by spotting them on Sc-His media containing 0-30 mM 3-Amino-1,2,4-triazole (3-AT)
647 (A8056, Sigma-Aldrich, USA). The minimum concentration of 3-AT that completely inhibits
648 the growth of the bait was considered for the Y1H screen/ assay. For the mating-based Y1H
649 screen, the diploids generated by mating were resuspended in sterile 96-well plates containing
650 Sc-Trp-His media and allowed to grow in shaking incubators for 24 hrs at 30ºC. After 24 hrs
651 of growth, OD was measured. Volumes corresponding to equal OD were spotted on Sc-Trp-
652 His+3AT media, incubated at 30ºC, and scored for growth on days 3-5 post-incubation. Spots
653 containing at least 5 colonies were considered positive for growth. For the Y1H screen, spots
654 showing growth on all three concentrations of 3-AT, i.e., 20, 25, and 30 mM by day 5, or
655 growth on 20 and 25 mM 3-AT by day 3 were considered positive for binding. For the co-
656 transformation-based Y1H assay, yeast baits were transformed with TF encoding plasmids and
657 selected on Sc-Trp-His media. Following selection, the cells were resuspended in Sc-Trp-His
658 media and allowed to grow in shaking incubators for 24 hrs at 30ºC. After 24 hrs of growth,
659 OD was measured. Volumes corresponding to equal OD were spotted on Sc-Trp-His media
660 with respective concentrations of 3-AT and incubated at 30ºC.The plates were inspected for
661 growth and imaged over days 3- 5 post-incubation.
662
663 **Plant materials**
664 *Arabidopsis thaliana* ecotype Columbia-0 (Col-0) was used as the wild-type control. All the
665 lines used in this study are in Col-0 genetic background. The genotypes used in this study are
666 described in **S6 Table**. The genotypes *cuc2-1* and *pBLS>>miR319a* (Originally in L*er*; Efroni
667 et al., 2008; Hasson et al., 2011) was brought into the Col-0 background by back crossing three
668 times. *pMIR319C::GUS*$^{\#1}$ (Nag et al., 2009) was established in various mutant backgrounds by
669 crossing and was confirmed by GUS assays in the F3/F4 generation. *cuc2-3;miR319c-1*,
670 *cuc2-3;miR319ab* and *miR319abc* mutants were generated by crossing respective mutant lines
671 *cuc2-3* (Nikovics et al., 2006), *miR319ab* (Koyama et al., 2017), *miR319c-1* (SAIL_647_B03/
672 CS827925) and confirmed by genotyping in F3 generation. *cuc2-1;GR*$^{\#2}$ was established by

673 crossing *cuc2-1* and Col-0;*GR*$^{\#2}$ (Shankar et al., 2023) mutants and confirmed by phenotyping
674 in F3 generation. All genotyping primers are listed in **S5 Table**.
675
676 **Plant growth condition and chemical treatments**
677 For GUS assays and phenotyping experiments, seeds were surface-sterilized with 0.05% SDS
678 containing 70% ethanol solution for 10 min, followed by wash with 100% ethanol twice and
679 sown on 1X Murashige and Skoog (MS), 0.8% agar medium (PT011, HiMedia Laboratories,
680 India) containing 0.025% ethanol (Mock) or 6 μM dexamethasone (DEX) (D4902, Sigma-
681 Aldrich, USA). After sowing, seeds were kept for stratification for three days in the dark at
682 4°C and then shifted to a plant growth chamber (I-41LL, Percival Scientific, USA) set at 22°C,
683 60% relative humidity, long-day conditions (16h/8h light/dark period, 100 $\mu mol.m^{-2}.s^{-1}$). 14-
684 day old seedlings were transplanted onto a soil mixture containing Soilrite and Perlite (Keltech
685 Energies, India) in a 3:1 ratio. Plants were grown till maturity in growth rooms with the
686 conditions as described for growth chamber.

687 For transient DEX and cycloheximide (CHX) treatments, 9 day-old mock (1X MS, 0.8% agar
688 medium containing 0.025% ethanol) grown seedlings were transferred onto petri dishes filled
689 with 0.5X MS medium, supplemented with 1% sucrose, 1X Gamborg B5 vitamins (PL018,
690 HiMedia Laboratories, India), 12 μM DEX, and/or 10 μM CHX (C7698, Sigma-Aldrich,
691 USA), incubated for 2 hours and harvested under liquid N2 prior to RNA isolation. In the case
692 of phenotyping experiment to study embryonic and cotyledon defects in *cuc2-1;GR*$^{\#2}$
693 seedlings, 14 day old mock-grown *cuc2-1;GR*$^{\#2}$ seedlings were transferred onto soil mixture
694 (as described earlier) and incubated in growth rooms until bolting stage (growth conditions as
695 described for growth chamber). Upon bolting, plants were sprayed with 12 μM DEX solution
696 on alternate days until seed harvest.

697 For confocal imaging experiments, seeds were stratified in the dark for two days at 4°C to
698 synchronize germination. Plants were grown on petri dishes filled with 0.5X MS medium,
699 supplemented with 0.8% agar, 1% sucrose, and 0.1% Plant Protective Mixture (Plant Cell
700 Technology) in a growth chamber under long-day conditions (16h/8h light/dark period, 95
701 $\mu mol.m^{-2}.s^{-1}$) at 22 ± 1°C with 60-70% relative humidity.

702

703

704 **DNA constructs and transgenic line generation**

705 For the generation of *pMIR319C* deletion and *mCUCBSpMIR319C::GUS* constructs, a 2.7 kb
706 genomic fragment corresponding to the *MIR319C* URR from the start of pre-*MIR319C* was
707 amplified from Col-0 genomic DNA using Phusion High Fidelity DNA polymerase (M0530,
708 New England Biolabs, USA) and cloned into modified *P4P1R* entry vector (a kind gift from
709 Ram Yadav, IISER Mohali, India) by gateway BP reaction (11789020, Invitrogen, USA) to
710 generate the *pMIR319C-P4P1R* construct. To introduce mutation at the CUC-binding site, we
711 utilized a PCR-based site directed mutagenesis approach. Briefly, forward, and reverse primers
712 carrying mutations in CUC-binding site (mCUCBS) was first used in a PCR reaction with
713 *pMIR319C-P4P1R* template using Phusion DNA polymerase. Post PCR reaction, the product
714 was digested with *Dpn*I (R0176, New England Biolabs, USA) and transformed into *E. coli* and
715 selected on LB agar containing 100 mg/l ampicillin. Plasmids were purified from resulting
716 colonies using QIAprep Spin Miniprep Kit (Qiagen, Germany) and mCUCBS was confirmed
717 by Sanger sequencing. The entry clone *mCUCBSpMIR319C-P4P1R* was recombined into
718 *R4L1pGWB532* destination vector (Gift from Tsuyoshi Nakagawa, Shimane University, Japan)
719 by LR reaction (11791020, Invitrogen, USA) to generate the *mCUCBSpMIR319C::GUS*
720 construct. Sequence information of primers used to generate the constructs are provided in the
721 **S5 Table**.

722 *mCUCBSpMIR319C::GUS* construct was integrated into Col-0 background by the
723 *Agrobacterium tumefaciens*-mediated floral dip method (Clough and Bent, 1998) except Silwet
724 L-77 was used at a concentration of 50 µl/litre. Following transformation, seeds were harvested
725 and screened for the ability to grow on MS media in presence of 20 mg/l hygromycin. At least
726 five independent lines were established for each construct and confirmed by genotyping in T3
727 generation. Sequence information of primers used for genotyping are provided in the **S5 Table**.
728

729 **β-glucuronidase (GUS) assay**

730 GUS assays were performed as described earlier (Shankar et al., 2023). Briefly, samples were
731 collected in ice-cold 90% acetone, incubated at room temperature for 20 min, followed by
732 washing with ice-cold staining buffer (50 mM sodium phosphate, pH 7.0, 0.2% Triton X-100,
733 5 mM potassium ferrocyanide, and 5 mM potassium ferricyanide). Fresh staining buffer was
734 added with 2 mM X-Gluc (R0851, Thermo Scientific, USA) and incubated overnight at 37°C
735 in dark. Staining buffer was replaced with 70% ethanol, and 70% ethanol was changed 3-4

736 times in regular intervals to clear the tissue. Shoot apices and leaf primordia were dissected
737 and mounted on a glass slide containing lactic acid under the microscope and were imaged
738 using Olympus BX51 trinocular DIC microscope fitted with ProgResC3 camera and
739 ProgResCapture Pro2.6 software (Jenoptik, Germany) with the following settings, exposure-
740 65ms, brightness-10 units, contrast- 35 units, colour temperature- 5000K, image resolution-
741 (1040 x 770 2X Bin), while keeping all other settings in default mode.
742
743 **GUS domain, leaf area and pavement cell area quantification**
744 The extent of reporter gene expression in the *pMIR319C::GUS* and *mCUCBSpMIR319C::GUS*
745 transgenic lines were determined using a pixel density quantification method reported in
746 Shankar et al., 2023. Images of 6 and 9-day old seedlings were captured using LEICA EZ4 E
747 stereomicroscope equipped with LAS EZ software. Areas of the dissected mature first pair of
748 leaves from 25-day old plants were determined using the polygon selection tool of the ImageJ
749 software. For pavement cell area measurements, dissected mature first pair of leaves were first
750 incubated in 7:1 absolute ethanol: glacial acetic acid clearing solution. After 24 hours, clearing
751 solution was replaced with 1M KOH solution for 30 minutes, washed twice with sterile water
752 and incubated in 37% D-lactic acid solution until tissue became completely transparent. The
753 clarified leaf samples were mounted on a glass slide using D-lactic acid and imaged using
754 Olympus BX51 trinocular DIC microscope fitted with ProgResC3 camera and ProgResCapture
755 Pro2.6 software (Jenoptik, Germany) with similar settings as described earlier. Cell areas were
756 determined using the polygon selection tool of the ImageJ software.
757
758 **Confocal microscopy and imaging**
759 For imaging of the first pair of leaf, one cotyledon was removed using fine tweezers or an
760 injection needle from two-day-old plants to expose the initiating leaf primordium for imaging
761 of leaf at 1 day after initiation (DAI). The seedlings were stained with 1 mg/mL Propidium
762 Iodide (PI) solution for 2-3 minutes and then were rinsed with water. The dissected plants then
763 were placed horizontally in Ø60 mm Petri dishes filled with 0.5X MS medium, supplemented
764 with 1.5% agar, 1% sucrose, and 0.1% Plant Protective Mixture (Plant Cell Technology). Plants
765 were immersed in water containing 0.1% PPM for imaging. Three to four replicates were
766 imaged using the PI staining and at least half of the abaxial leaf surface was imaged at 1 DAI,
767 3 DAI and 5 DAI respectively.
768

769 All confocal imaging was performed with an LSM980 upright confocal microscope using a
770 long-distance water-dipping objective (AP 20X/1.0; Zeiss) at the confocal facility of
771 MechanoDevo team (RDP, ENS de Lyon). Excitation was performed using a diode laser with
772 561 nm for PI. Images were collected at 580-650 nm for PI with a GAsP detector and a beam
773 splitter operating at 488 and 561 nm. Confocal stacks were acquired at 512x512 resolution and
774 16-bit image depth, with 1.4 µm distance in Z-dimension. For samples larger than the field of
775 view, multiple overlapping stacks were obtained and later stitched together using
776 MorphoGraphX (Barbier de Reuille et al., 2015; Strauss et al., 2022).
777

778 **Confocal Image analysis**

779 Cellular growth and expression quantifications were conducted using MorphoGraphX. Stacks
780 were processed as described previously (Le Gloanec et al., 2022). After digitally removing the
781 trichomes when necessary, the organ surface was detected with the 'Edge detect' tool with a
782 threshold of 20000 with 'closing' to fill holes, followed by the 'Edge detect angle' (10000). An
783 initial 5 µm cube size mesh was then created and subdivided three times before projecting the
784 membrane signal (2-5 µm). Cell segmentation was performed manually. Metrics such as area
785 cell size were computed as described before (Barbier de Reuille et al., 2015; Sapala et al.,
786 2018).

787

788 **RNA isolation and RT-qPCR**

789 Total RNA was extracted using the TRIzol method described earlier (Challa et al., 2016). 10
790 µg of RNA was used for DNase (EN0521, Thermo Scientific, USA) treatment. 1.5 µg DNase-
791 treated RNA was converted to cDNA using RevertAid Reverse Transcriptase (EP0441,
792 Thermo Scientific, USA) and 2.5 µM oligo dT according to the manufacturer's instructions.
793 Quantitative PCR reactions with 25 ng cDNA and 0.4 µM primers were set up using the
794 DyNAmo Flash SYBR Green RT-qPCR kit (F415L, Thermo Scientific, USA), according to
795 the manufacturer's instructions. 10 µl qPCR reactions were carried out in QuantStudio™ 6
796 Flex Real-Time PCR System, 384-well format (Applied Biosystems, USA). Results were
797 analyzed using the inbuilt QuantStudio6 Pro software, and ΔΔCT values were determined after
798 normalization with *PROTEIN PHOSPHATASE 2A SUBUNIT A3 (PP2AA3*). Relative fold
799 changes in transcript levels were calculated using the formula $2^{-\Delta\Delta CT}$. All primer sequences are
800 provided in **S5 Table**.
801

802 **Statistical analysis**

803 All graphical representations and statistical analysis were performed using GraphPad Prism 9
804 software (GraphPad, USA). First, samples were tested for Gaussian distribution using the
805 Shapiro-Wilk normality test. If samples were normally distributed, pairwise comparisons were
806 performed using unpaired *t*-test. Welch's correction was applied if variances were different
807 among the samples. Statistical differences among multiple genotypes were determined by
808 ordinary One-Way ANOVA followed by Tukey's multiple comparisons test or One-Way
809 ANOVA followed by Dunnet's T3 post-hoc test, depending on whether variances were
810 significantly different among the genotypes. If the samples failed the normality test, then
811 pairwise comparisons were carried out by Mann Whitney test. Statistical differences among
812 multiple genotypes were determined by One-Way ANOVA followed by Dunn's post-hoc test.
813 To compare statistical differences among multiple genotypes subjected to ethanol (Mock) or
814 dexamethasone (DEX) treatments, we used Two-Way ANOVA followed by Tukey's post-hoc
815 test. *p*-values obtained from the respective tests are indicated above the data bars in several
816 plots. For plots with a large number of comparisons, statistical differences among samples are
817 indicated by different alphabets.

818

819 ## References

820

821 **Aida M, Ishida T, Fukaki H, Fujisawa H, Tasaka M** (1997) Genes involved in organ separation in
822 Arabidopsis: An analysis of the cup-shaped cotyledon mutant. Plant Cell **9**: 841–857
823 **Aida M, Ishida T, Tasaka M** (1999) Shoot apical meristem and cotyledon formation during
824 Arabidopsis embryogenesis: interaction among the CUP-SHAPED COTYLEDON and SHOOT
825 MERISTEMLESS genes. Development **126**: 1563–1570
826 **Aida M, Tsubakimoto Y, Shimizu S, Ogisu H, Kamiya M, Iwamoto R, Takeda S, Karim MR,**
827 **Mizutani M, Lenhard M, et al** (2020) Establishment of the embryonic shoot meristem involves
828 activation of two classes of genes with opposing functions for meristem activities. Int J Mol Sci **21**:
829 1–16
830 **Anastasiou E, Kenz S, Gerstung M, MacLean D, Timmer J, Fleck C, et al** (2007) Control of Plant
831 Organ Size by KLUH/CYP78A5-Dependent Intercellular Signaling. Dev Cell 13: 843–56
832 **Andriankaja M, Dhondt S, DeBodt S, Vanhaeren H, Coppens F, DeMilde L, Mühlenbock P,**
833 **Skirycz A, Gonzalez N, Beemster GTS, et al** (2012) Exit from Proliferation during Leaf
834 Development in Arabidopsis thaliana: A Not-So-Gradual Process. Dev Cell **22**: 64–78
835 **Bar M, Ori N** (2014) Leaf development and morphogenesis. Development **141**: 4219–4230
836 **Barbier de Reuille P, Routier-Kierzkowska A.L, Kierzkowski D, Bassel GW, Schüpbach T,**
837 **Tauriello G, Bajpai N, Strauss S, Weber A, Kiss A** et al (2015). MorphoGraphX: A platform for
838 quantifying morphogenesis in 4D. Elife **4**: 05864
839 **Barton MK** (2010) Twenty years on: The inner workings of the shoot apical meristem, a
840 developmental dynamo. Dev Biol **341**: 95–113

841 **Bilsborough GD, Runions A, Barkoulas M, Jenkins HW, Hasson A, Galinha C, Laufs P, Hay A,**
842 **Prusinkiewicz P, Tsiantis M** (2011) Model for the regulation of Arabidopsis thaliana leaf margin
843 development. Proc Natl Acad Sci U S A **108**: 3424–3429
844 **Challa KR, Aggarwal P, Nath U** (2016) Activation of *YUCCA5* by the Transcription Factor TCP4
845 Integrates Developmental and Environmental Signals to Promote Hypocotyl Elongation in
846 Arabidopsis. Plant Cell **28**: 2117–2130
847 **Challa KR, Rath M, Nath U** (2019) The CIN-TCP transcription factors promote commitment to
848 differentiation in Arabidopsis leaf pavement cells via both auxin-dependent and independent
849 pathways. PLoS Genet **15**: 1–30
850 **Challa KR, Rath M, Sharma AN, Bajpai AK, Davuluri S, Acharya KK, Nath U** (2021) Active
851 suppression of leaflet emergence as a mechanism of simple leaf development. Nat Plants **7**: 1264–
852 1275
853 **Clough SJ, Bent AF** (1998). Floral dip: A simplified method for Agrobacterium-mediated
854 transformation of Arabidopsis thaliana. Plant J **16**: 735–43
855 **Donnelly PM, Bonetta D, Tsukaya H, Dengler RE, Dengler NG** (1999) Cell cycling and cell
856 enlargement in developing leaves of Arabidopsis. Dev Biol **215**: 407–419
857 **Du F, Guan C, Jiao Y** (2018) Molecular Mechanisms of Leaf Morphogenesis. Mol Plant **11**: 1117–
858 1134
859 **Efroni I, Blum E, Goldshmidt A, Eshed Y** (2008) A Protracted and Dynamic Maturation Schedule
860 Underlies Arabidopsis Leaf Development. the Plant Cell Online **20**: 2293–2306
861 **Fox S, Southam P, Pantin F, Kennaway R, Robinson S, Castorina G, Sánchez-Corrales YE,**
862 **Sablowski R, Chan J, Grieneisen V, et al** (2018) Spatiotemporal coordination of cell division and
863 growth during organ morphogenesis. PLoS Biol **16**: e2005952
864 **Fuxman Bass JI, Pons C, Kozlowski L, Reece-Hoyes JS, Shrestha S, Holdorf AD,** et al (2016). A
865 gene-centered C. elegans protein–DNA interaction network provides a framework for functional
866 predictions. Mol Syst Biol **12**: 884
867 **Gázquez A, Beemster GTS** (2017) What determines organ size differences between species? A meta-
868 analysis of the cellular basis. New Phytologist **215**: 299–308
869 **Gonzalez N, Vanhaeren H, Inzé D** (2012) Leaf size control: Complex coordination of cell division
870 and expansion. Trends Plant Sci **17**: 332–340
871 **Hasson A, Plessis A, Blein T, Adroher B, Grigg S, Tsiantis M, Boudaoud A, Damerval C, Laufs**
872 **P** (2011) Evolution and diverse roles of the CUP-SHAPED COTYLEDON genes in Arabidopsis leaf
873 development. Plant Cell **23**: 54–68
874 **Hepworth J, Lenhard M** (2014) Regulation of plant lateral-organ growth by modulating cell number
875 and size. Curr Opin Plant Biol **17**: 36–42
876 **Hibara KI, Karim MR, Takada S, Taoka KI, Furutani M, Aida M, Tasaka M** (2006) Arabidopsis
877 CUP-SHAPED COTYLEDON3 regulates postembryonic shoot meristem and organ boundary
878 formation. Plant Cell **18**: 2946–2957
879 **Hisanaga T, Kawade K, Tsukaya H** (2015) Compensation: A key to clarifying the organ-level
880 regulation of lateral organ size in plants. J Exp Bot **66**: 1055–1063
881 **Horiguchi G, Kim GT, Tsukaya H** (2005) The transcription factor AtGRF5 and the transcription
882 coactivator AN3 regulate cell proliferation in leaf primordia of Arabidopsis thaliana. Plant Journal **43**:
883 68–78
884 **Ishida T, Aida M, Takada S, Tasaka M** (2000) Involvement of CUP-SHAPED COTYLEDON
885 genes in gynoecium and ovule development in Arabidopsis thaliana. Plant Cell Physiol **41**: 60–67
886 **Kalve S, De Vos D, Beemster GTS** (2014) Leaf development: a cellular perspective. Front Plant Sci
887 **5**: 1–25

Kazama T, Ichihashi Y, Murata S, Tsukaya H (2010). The mechanism of cell cycle arrest front progression explained by a KLUH/CYP78A5-dependent mobile growth factor in developing leaves of arabidopsis thaliana. Plant Cell Physiol **51**:1046–54

Kicheva A, Briscoe J (2023) Control of Tissue Development by Morphogens. Annu Rev Cell Dev Biol 2023 **39**: 2023

Koyama T, Furutani M, Tasaka M, Ohme-Takagi M (2007) TCP Transcription Factors Control the Morphology of Shoot Lateral Organs via Negative Regulation of the Expression of Boundary-Specific Genes in Arabidopsis. Plant Cell **19**: 473–484

Koyama T, Mitsuda N, Seki M, Shinozaki K, Ohme-Takagi M (2010) TCP transcription factors regulate the activities of ASYMMETRIC LEAVES1 and miR164, as well as the auxin response, during differentiation of leaves in Arabidopsis. Plant Cell **22**: 3574–3588

Koyama T, Sato F, Ohme-Takagi M (2017) Roles of miR319 and TCP transcription factors in leaf development. Plant Physiol **175**: 874–885

Larue CT, Wen J, Walker JC (2009) A microRNA-transcription factor module regulates lateral organ size and patterning in Arabidopsis. Plant Journal **58**: 450–463

Laufs P, Peaucelle A, Morin H, Traas J (2004) MicroRNA regulation of the CUC genes is required for boundary size control in Arabidopsis meristems. Development **131**: 4311–4322

Le Gloanec C, Collet L, Silveira SR, Wang B, Routier-Kierzkowska AL, and Kierzkowski D (2022). Cell type-specific dynamics underlie cellular growth variability in plants. Development **149**: dev200783.

Li Y, Xia T, Gao F, Li Y (2020) Control of plant branching by the CUC2/CUC3-DA1-UBP15 regulatory module. Plant Cell **32**: 1919–1932

Lindemose S, Jensen MK, De Velde J Van, O'Shea C, Heyndrickx KS, Workman CT, Vandepoele K, Skriver K, Masi F De (2014) A DNA-binding-site landscape and regulatory network analysis for NAC transcription factors in Arabidopsis thaliana. Nucleic Acids Res **42**: 7681–7693

Maugarny-Calès A, Cortizo M, Adroher B, Borrega N, Gonçalves B, Brunoud G, Vernoux T, Arnaud N, Laufs P (2019) Dissecting the pathways coordinating patterning and growth by plant boundary domains. PLoS Genet **15**: 1–30

Maugarny-Calès A, Laufs P (2018) Getting leaves into shape: A molecular, cellular, environmental and evolutionary view. Development **145**: dev161646

Meinhardt H (2009) Models for the generation and interpretation of gradients. Cold Spring Harb Perspect Biol **1**: a001362

Nag A, King S, Jack T (2009) miR319a targeting of TCP4 is critical for petal growth and development in Arabidopsis. Proceedings of the National Academy of Sciences **106**: 22534–22539

Nakata M, Matsumoto N, Tsugeki R, Rikirsch E, Laux T, Okada K (2012) Roles of the middle domain-specific WUSCHEL-RELATED HOMEOBOX genes in early development of leaves in Arabidopsis. Plant Cell **24**: 519–535

Nikovics K, Blein T, Peaucelle A, Ishida T, Morin H, Aida M, Laufs P (2006) The balance between the MIR164A and CUC2 genes controls leaf margin serration in Arabidopsis. Plant Cell **18**: 2929–2945

Ooka H, Satoh K, Doi K, Nagata T, Otomo Y, Murakami K, Matsubara K, Osato N, Kawai J, Carninci P, et al (2003) Comprehensive Analysis of NAC Family Genes in Oryza sativa and Arabidopsis thaliana. DNA Research **10**: 239–247

Palatnik JF, Allen E, Wu X, Schommer C, Schwab R, Carrington JC, Weigel D (2003) Control of leaf morphotgenesis by microRNAs. Nature **425**: 257–263

Pruneda-Paz, JL, Breton, G, Nagel, DH, Kang, SE, Bonaldi, K, Doherty, CJ, Ravelo, S, Galli, M, Ecker, JR, and Kay, SA (2014). A Genome-Scale Resource for the Functional Characterization of Arabidopsis Transcription Factors. Cell Rep. **8**: 622–632

936 **Rodriguez RE, Mecchia MA, Debernardi JM, Schommer C, Weigel D, Palatnik JF** (2010)
937 Control of cell proliferation in Arabidopsis thaliana by microRNA miR396. Development 137:103–12
938 **Rodriguez RE, Debernardi JM, Palatnik JF** (2014) Morphogenesis of simple leaves: Regulation of
939 leaf size and shape. Wiley Interdiscip Rev Dev Biol 3: 41–57
940 **Rubio-Somoza I, Zhou CM, Confraria A, Martinho C, Von Born P, Baena-Gonzalez E, Wang**
941 **JW, Weigel D** (2014) Temporal control of leaf complexity by miRNA-regulated licensing of protein
942 complexes. Current Biology **24**: 2714–2719
943 **Sapala, A, Runions A, Routier-Kierzkowska AL, Gupta MD, Hong L, Hofhuis H, Verger S,**
944 **Mosca G, Li CB, Hay A** et al (2018). Why plants make puzzle cells, and how their shape emerges.
945 Elife **7**: e32794.
946 **Sarojam R, Sappl PG, Goldshmidt A, Efroni I, Floyd SK, Eshed Y, Bowmana JL** (2010)
947 Differentiating Arabidopsis shoots from leaves by combined YABBY activities. Plant Cell **22**: 2113–
948 2130
949 **Sarvepalli K, Das Gupta M, Challa KR, Nath U** (2019) Molecular cartography of leaf
950 development — role of transcription factors. Curr Opin Plant Biol **47**: 22–31
951 **Sarvepalli K, Nath U** (2018) CIN-TCP transcription factors: Transiting cell proliferation in plants.
952 IUBMB Life **70**: 718–731
953 **Schneider M, Van Bel M, Inzé D, Baekelandt A** (2024) Leaf growth – complex regulation of a
954 seemingly simple process. Plant Journal **117**: 1018–1051
955 **Scofield S, Murison A, Jones A, Fozard J, Aida M, Band LR, Bennett M, Murray JAH** (2018)
956 Coordination of meristem and boundary functions by transcription factors in the SHOOT
957 MERISTEMLESS regulatory network. Development **145**: dev157081
958 **Shankar N, Sunkara P, Nath U** (2023) A double-negative feedback loop between miR319c and
959 JAW-TCPs establishes growth pattern in incipient leaf primordia in Arabidopsis thaliana. PLoS Genet
960 **19**: 1–25
961 **Shleizer-Burko S, Burko Y, Ben-Herzel O, Ori N** (2011) Dynamic growth program regulated by
962 LANCEOLATE enables flexible leaf patterning. Development **138**: 695–704
963 **Sieber P, Wellmer F, Gheyselinck J, Riechmann JL, Meyerowitz EM** (2007) Redundancy and
964 specialization among plant microRNAs: Role of the MIR164 family in developmental robustness.
965 Development **134**: 1051–1060
966 **Strauss, S, Runions A, Lane B, Eschweiler D, Bajpai N, Trozzi N, Routier-Kierzkowska AL,**
967 **Yoshida S, Rodrigues da Silveira S, Vijayan A** et al (2022). Using positional information to
968 provide context for biological image analysis with MorphoGraphX 2.0. Elife **11**: e72601
969 **Takeda S, Hanano K, Kariya A, Shimizu S, Zhao L, Matsui M, Tasaka M, Aida M** (2011) CUP-
970 SHAPED COTYLEDON1 transcription factor activates the expression of LSH4 and LSH3, two
971 members of the ALOG gene family, in shoot organ boundary cells. Plant Journal **66**: 1066–1077
972 **Tian C, Zhang X, He J, Yu H, Wang Y, Shi B, Han Y, Wang G, Feng X, Zhang C,** et al (2014).
973 An organ boundary-enriched gene regulatory network uncovers regulatory hierarchies underlying
974 axillary meristem initiation. Mol Syst Biol **10**: 755
975 **Tian, C., Wang, Y., Yu, H., He, J., Wang, J., Shi, B., Du, Q., Provart, N.J., Meyerowitz, E.M.,**
976 **and Jiao, Y** (2019). A gene expression map of shoot domains reveals regulatory mechanisms. Nat.
977 Commun **10**: 1–12.
978 **Tsukaya H** (2005) Leaf shape: Genetic controls and environmental factors. International Journal of
979 Developmental Biology **49**: 547–555
980 **Tsukaya H** (2019) Re-examination of the role of endoreduplication on cell-size control in leaves. J
981 Plant Res **132**: 571–580
982 **Vercruysse J, Baekelandt A, Gonzalez N, Inzé D** (2021) Molecular networks regulating cell
983 division during Arabidopsis leaf growth. J Exp Bot **71**: 2365–2378

Vercruyssen L, Verkest A, Gonzalez N, Heyndrickx KS, Eeckhout D, Han SK, et al (2014) ANGUSTIFOLIA3 binds to SWI/SNF chromatin remodeling complexes to regulate transcription during Arabidopsis leaf development. Plant Cell 26: 210–29

Vroemen CW, Mordhorst AP, Albrecht C, Kwaaitaal MACJ, De Vries SC (2003) The CUP-SHAPED COTYLEDON3 gene is required for boundary and shoot meristem formation in Arabidopsis. Plant Cell **15**: 1563–1577

Wang Q, Hasson A, Rossmann S, Theres K (2016) Divide et impera: Boundaries shape the plant body and initiate new meristems. New Phytologist **209**: 485–498

Wu G, Lin W-C, Huang T, Scott Poethig R, Springer PS, Kerstetter RA (2008) KANADI1 regulates adaxial-abaxial polarity in Arabidopsis by directly repressing the transcription of ASYMMETRIC LEAVES2. Proc Natl Acad Sci U S A **105**:16392-7

Figures

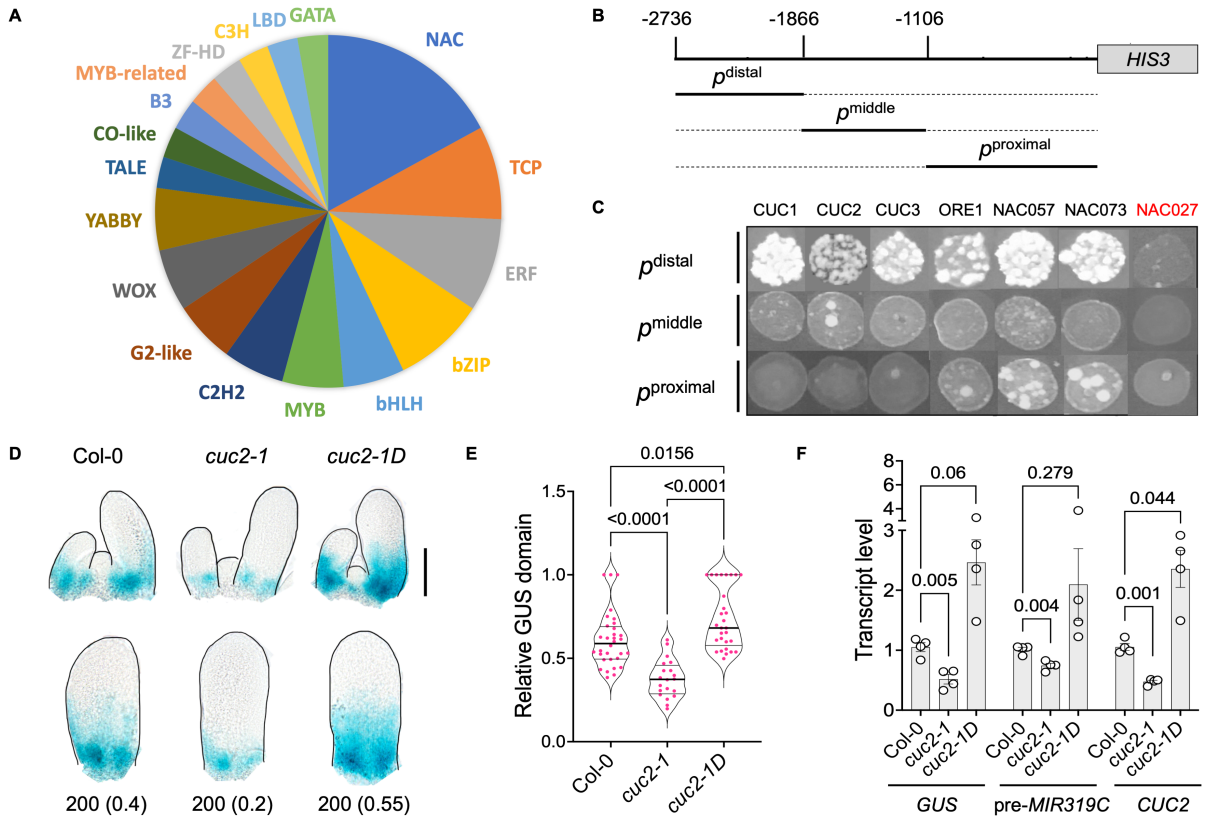

Figure 1: *MIR319C* expression in leaf primordia with altered *CUC2* levels. **(A)** Distribution of TF families (in %) recovered from the yeast one hybrid screen (Y1H) with 378 TFs and ~2.736 kb *MIR319C* URR. **(B)** Schematic representation of truncated *MIR319C* promoter fragments used for Y1H assay with NAC TFs. Grey box corresponds to *HIS3* CDS. The three horizontal lines below the URR scheme represent the truncated promoter regions, i.e., p^{distal} (-2736-1866), p^{middle} (-1866-1106) and $p^{proximal}$ (-1106), respectively. **(C)** Images of yeast growth harboring three different truncated *MIR319C* promoter regions upstream to the *HIS3* reporter gene and corresponding NAC TF preys as indicated, grown in the presence of inhibitory concentration of 3-AT. NAC027 served as negative control. **(D)** Bright field images of 10-day shoot apices (top panel) or 6th leaf primordia (bottom panel) of the indicated genotypes expressing *pMIR319C::GUS* transgene. Numbers below the leaf primordia images indicate leaf lengths and GUS domain/leaf length ratios are indicated within the parenthesis. Scale bar,100 µm. **(E)** Violin plots displaying the quantification of *pMIR319C::GUS* domain/leaf length (Y-

axis) in the genotypes indicated on the X-axis. Differences among samples are indicated by *p*-values on top of the comparisons, One-way ANOVA, Dunnett's post hoc test. N=20-32. **(F)** Quantification of *GUS,* pre-*MIR319C* and *CUC2* transcript in genotypes indicated on the X-axis. Error bars represent SEM of four biological replicates. Multiple comparisons were performed using One-way ANOVA followed by Dunnett's post hoc test. *p*-values are shown above the data bars.

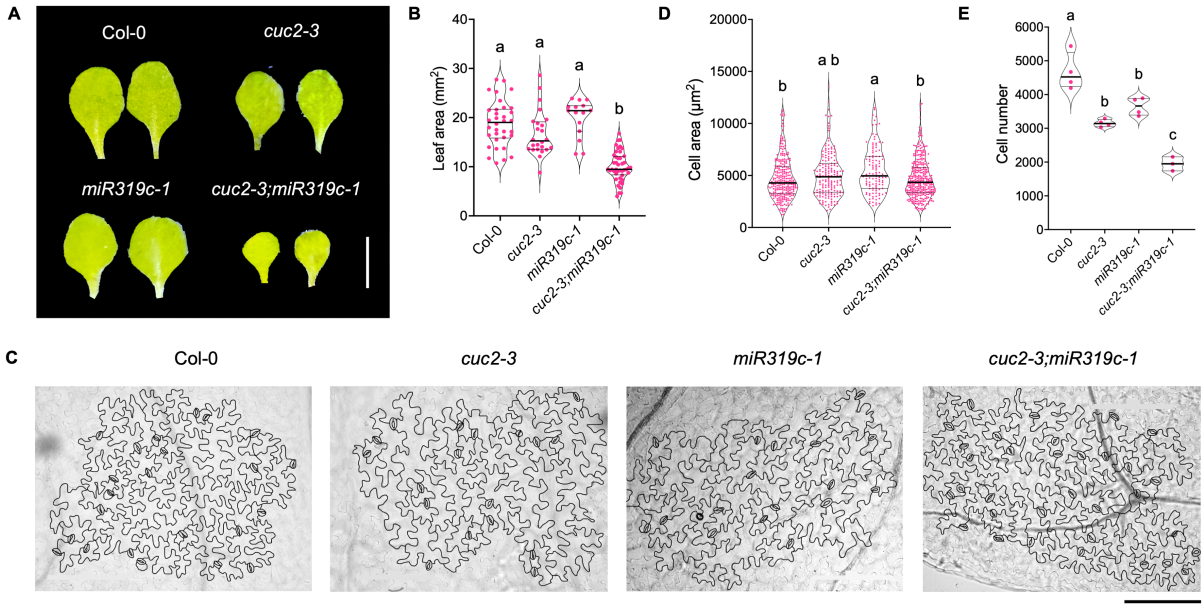

Figure 2: Role of *CUC2-MIR319C* module in leaf cell proliferation. (A) Representative images of mature first pair of leaves from 25-day old plants of the indicated genotypes. Scale, 5 mm. **(B)** Areas (Y-axis) of mature first pair of leaves of the indicated genotypes on the X-axis. N=15-44 leaves. Significant differences among the samples are indicated by different alphabets. p<0.0001. One-way ANOVA, followed by Dunn's multiple comparison test are performed to determine the significant differences among samples. **(C)** Representative images for pavement cell areas of mature first pair of leaves from 25-day old plants of the indicated genotypes. Pavement cells and stomata are outlined in black. Scale bar, 200 µm. **(D)** Distribution of pavement cell areas of mature first pair of leaves from 25-day old plants of the indicated genotypes (X-axis). N= 115-333 cells from 3-4 leaves. Significant differences among the samples are indicated by different alphabets. p<0.01. One-way ANOVA, followed by Dunn's multiple comparison test are performed to determine the significant differences among samples. **(E)** Cell numbers (Y-axis) in mature first pair of leaves of the indicated genotypes (X-axis). Cell number was determined as the ratio of leaf area by the average cell area for 3-4 leaves per genotype. Significant differences among the samples are indicated by different alphabets. p<0.01. One-way ANOVA, followed by Tukey's multiple comparison test are performed to determine the significant differences among samples.

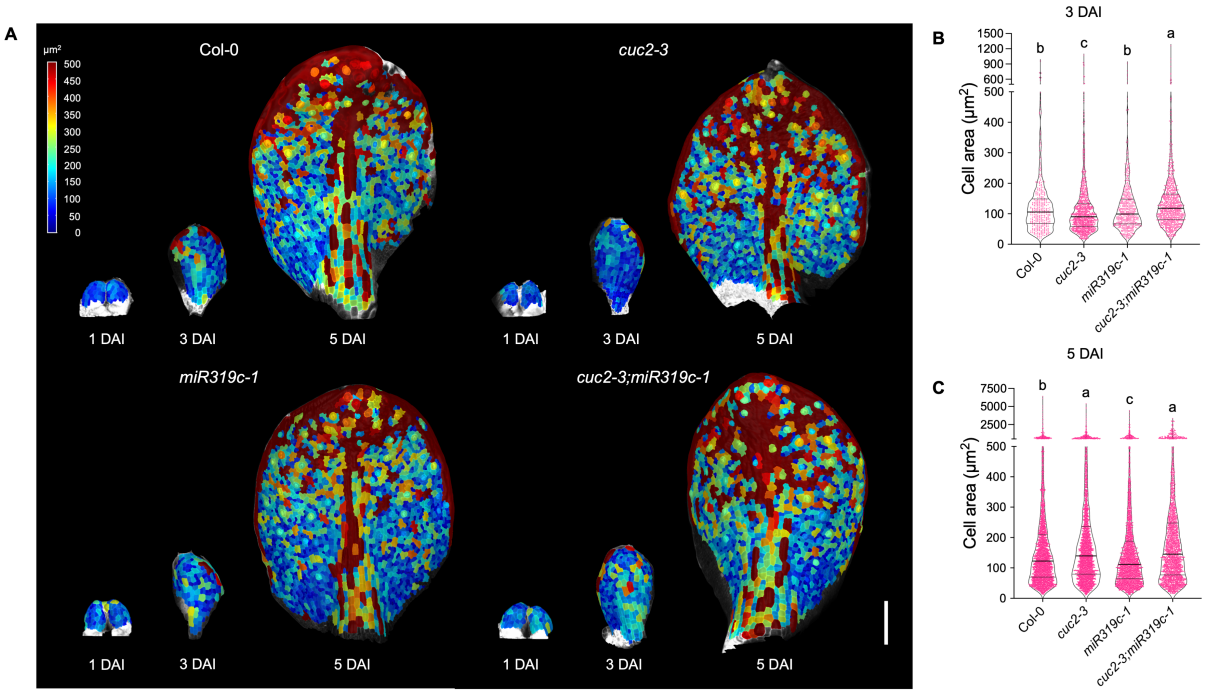

Figure 3: Cell proliferation pattern in leaf primordia with altered *CUC2* and *MIR319C* activities. **(A)** Heat maps of cell areas in the first pair leaf primordia at 1, 3, and 5 days after initiation (DAI) of the indicated genotypes. Scale, 100 µm. **(B)** Distribution of pavement cell areas of leaf primordia at 3 DAI of the indicated genotypes (X-axis). N= 380-1079 cells from 2-3 leaves. Significant differences among the samples are indicated by different alphabets. $p<0.05$. One-way ANOVA, followed by Dunn's multiple comparison test are performed to determine the significant differences among samples. **(C)** Distribution of pavement cell areas of leaf primordia at 5 DAI of the indicated genotypes (X-axis). N= 2435-3280 cells from 2-3 leaves. Significant differences among the samples are indicated by different alphabets. $p<0.01$. One-way ANOVA, followed by Dunn's multiple comparison test are performed to determine the significant differences among samples.

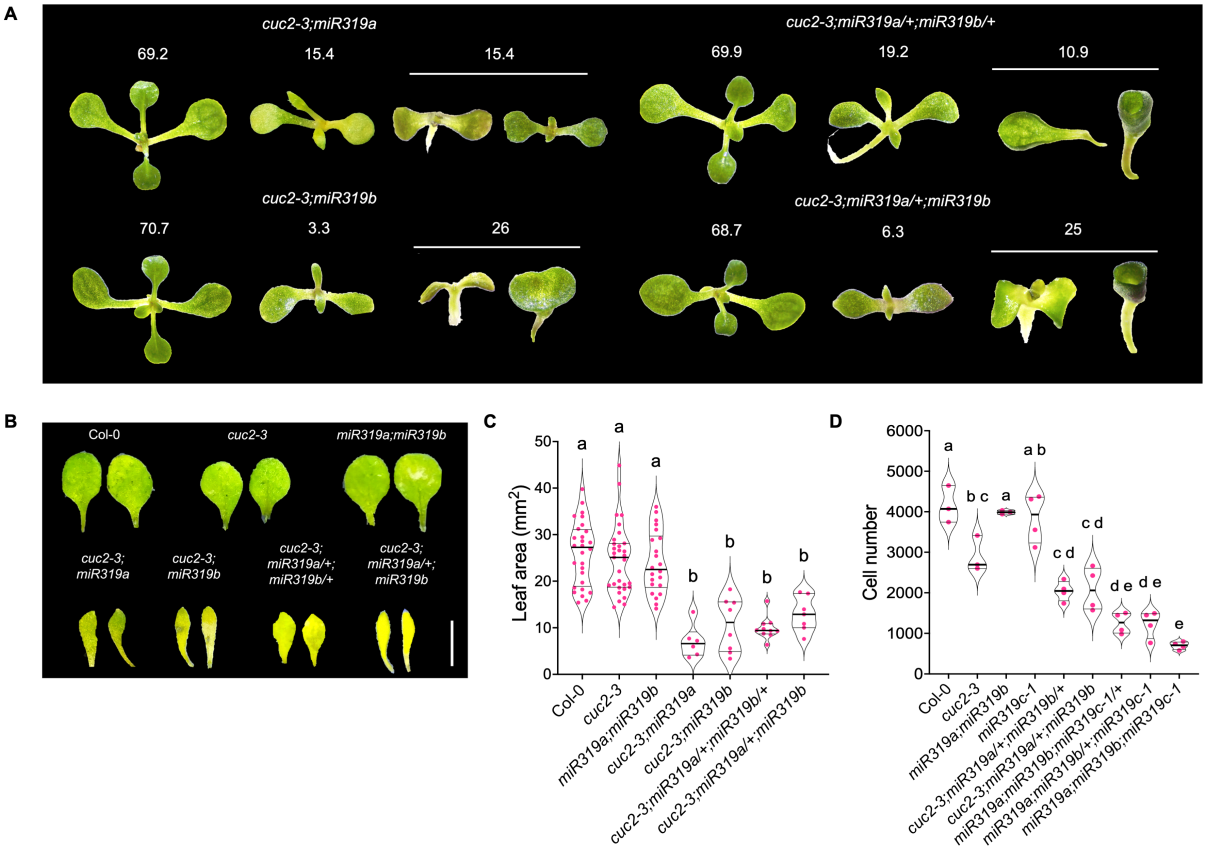

Figure 4: Genetic interaction between *CUC2* and *MIR319* genes in regulating pavement cell number during leaf growth. (A) Representative images of 9-day old seedlings for each of the three categories of phenotypes, i.e., wild-type, narrow leaves, and seedling arrest/cotyledon fusion observed in the *cuc2;miR319a;miR319b* mutant combinations. Numbers above the images denote the proportion (in %) of seedlings displaying the indicated phenotype. **(B)** Representative images of mature first pair of leaves from 25-day old plants of the indicated genotypes. Scale, 5 mm. **(C)** Areas (Y-axis) of mature first pair of leaves of the indicated genotypes (X-axis). N=6-31 leaves. Significant differences among the samples are indicated by different alphabets. $p<0.01$. One-way ANOVA, followed by Dunnett's T3 multiple comparison test are performed to determine the significant differences among samples. **(D)** Cell numbers (Y-axis) in mature first pair of leaves of the indicated genotypes (X-axis). Cell number was determined as the ratio of leaf area by the average cell area for 3-4 leaves per genotype. Significant differences among the samples are indicated by different alphabets. $p<0.05$. One-way ANOVA, followed by Tukey's multiple comparison test are performed to determine the significant differences among samples.

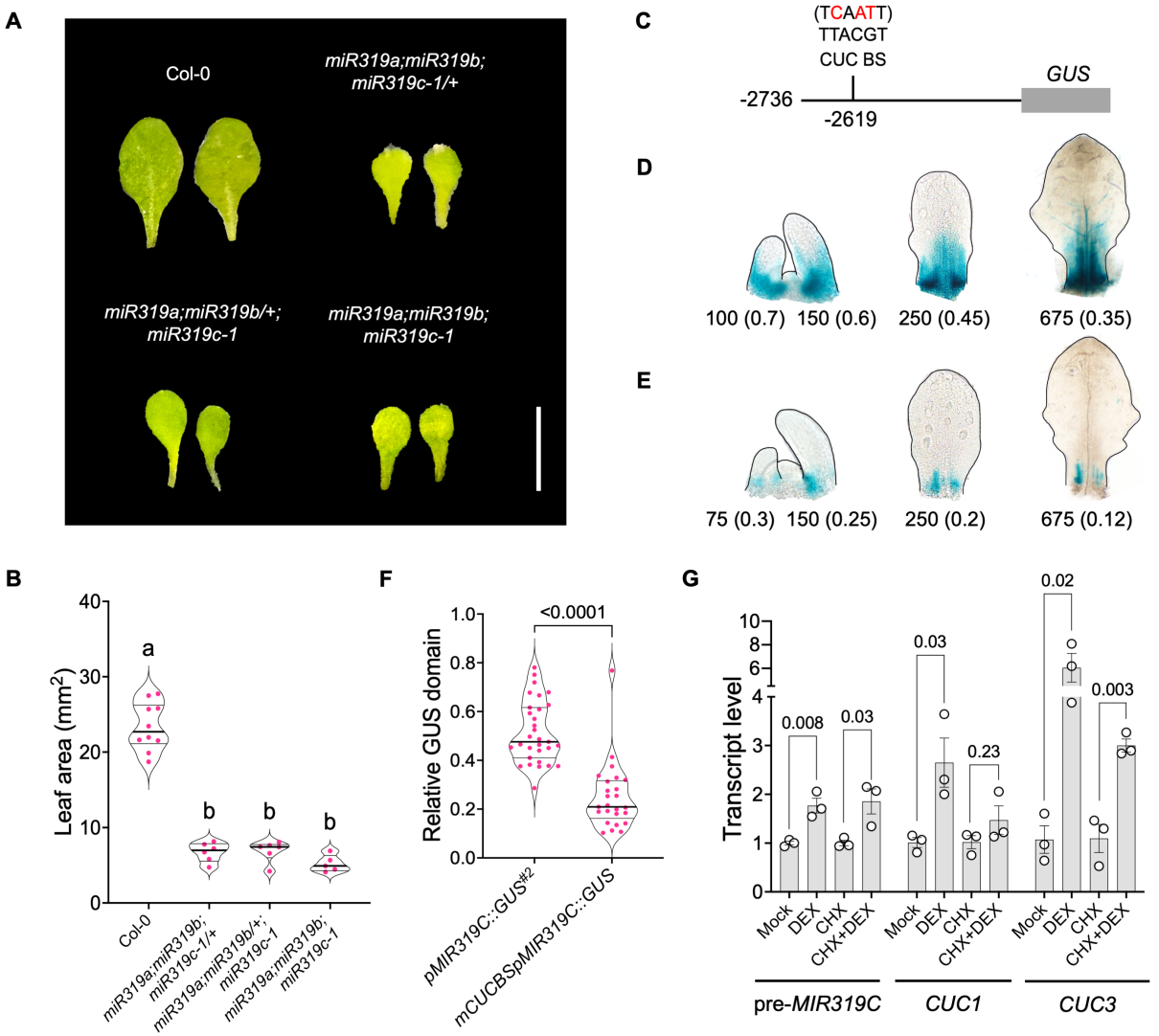

Figure 5: Genetic interaction between *MIR319* genes in regulating leaf size. (A) Representative images of mature first pair of leaves from 25-day old plants of the indicated genotypes. Scale, 5mm. **(B)** Areas (Y-axis) of mature first pair of leaves of the indicated genotypes (X-axis). N=4-10 leaves. Significant differences among the samples are indicated by different alphabets. p<0.0001. One-way ANOVA, followed by Dunnett's T3 multiple comparison test are performed to determine the significant differences among samples. **(C)** Schematic representation of the *MIR319C* promoter *GUS* construct with mutated bases on the CUC-binding site at the -2617, -2618, and -2620th nucleotide positions indicated in red. The *GUS* region is indicated by grey box. **(D-E)** Bright field images of shoot apices and 250, and 675 µm long leaf primordia on 6th, and 4th nodes respectively, expressing *GUS*-based reporter transgene under **(D)** *MIR319C* promoter or **(E)** *MIR319C* promoter carrying mutations on the CUC-binding site as indicated in **(C)**, respectively. **(F)** Violin plot displaying the quantification of *pMIR319C::GUS* or *mCUCBSpMIR319C::GUS* domain/leaf length in the 50-750 µm long leaf primordia on 4th-8th nodes. N=25 leaf primordia for *pMIR319C::GUS$^{\#2}$* and 31 leaf primordia for *mCUCBSpMIR319C::GUS*. Differences among samples are indicated by *p*-values on top of the comparisons, Unpaired *t*-test with Welch's correction for differences in variance. **(G)** Quantification of pre-*MIR319C*, *CUC1,* and *CUC3* transcript in 10-day old *pRPS5A::CUC2-GR-HA* seedlings treated for 2 hours with ethanol (Mock) or 12 µM dexamethasone (DEX) or 10 µM cycloheximide (CHX) or 10 µM cycloheximide and 12 µM dexamethasone (CHX+DEX) as indicated in the plot. Error bars represent SEM of three biological replicates. Pairwise comparisons were performed using unpaired *t*-test. *p*-values are shown above the data bars.

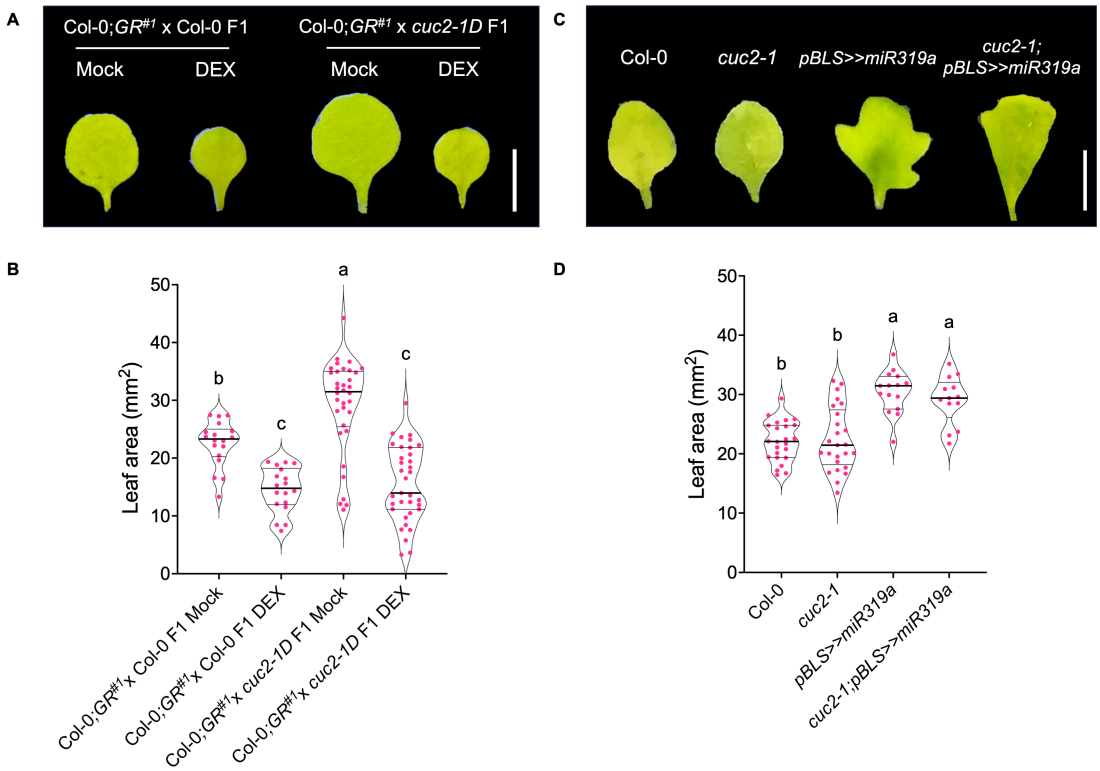

Figure 6: Effect of altered *CUC2* and *JAW-TCP* levels on leaf size. (A) Representative images of mature first leaves from 25-day old plants of the indicated genotypes and chemical treatments. Scale, 5 mm. **(B)** Areas (Y-axis) of mature first pair of leaves of the indicated genotypes and treatments (X-axis). N=18-35 leaves. Significant differences among samples are indicated by different lower-case alphabets. $p<0.01$, two-way ANOVA, Tukey's post hoc test was performed. **(C)** Representative images of first mature leaves from 25-day old plants of the indicated genotypes. Scale, 5 mm. **(D)** Areas (Y-axis) of mature first pair of leaves of the indicated genotypes (X-axis). N=12-25 leaves. Significant differences among the samples are indicated by different alphabets. $p<0.05$. One-way ANOVA, followed by Dunnett's T3 multiple comparison test are performed to determine the significant differences among samples.

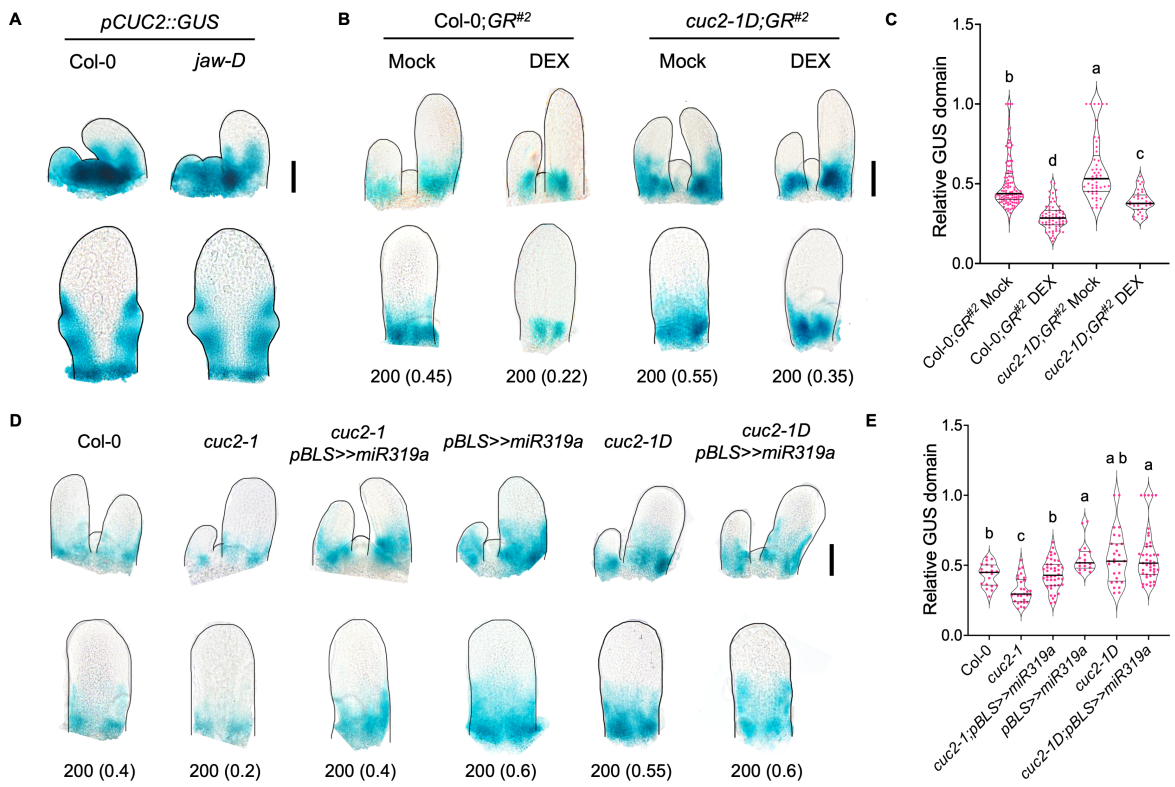

Figure 7: Regulation of *MIR319C* expression by *CUC2* and *JAW-TCP* genes in leaf primordia. **(A)** Bright field images of shoot apices (top panel) and 6th leaf primordia (bottom panel) from 10-day old Col-0 and *jaw-D* seedlings expressing *pCUC2::GUS* transgene. Scale bar, 50 µm. **(B)** Bright-field images of shoot apices (top panel) and 6th leaf primordia (bottom panel) dissected from 10-day old seedlings of indicated genotypes expressing the *pMIR319C::GUS* transgene. Scale bar, 50 µm. Numbers below the images represent leaf lengths in µm and those inside parenthesis denote the length of GUS domain relative to the leaf length. **(C)** Length of *pMIR319C::GUS* domain relative to total leaf length in 50-350 µm leaf primordia are plotted for the indicated genotypes. Differences among samples are indicated by different lower-case alphabets. $p<0.05$. N = 33-114. Two-way ANOVA, followed by Tukey's post hoc test are performed to determine the significant differences among samples. **(D)** Bright-field images of shoot apices (top panel) and 6th leaf primordia (bottom panel) dissected from 10-day old seedlings of indicated genotypes expressing the *pMIR319C::GUS* transgene. Scale bar, 50 µm. Numbers below the images represent leaf lengths in µm and those inside parenthesis denote the length of GUS domain relative to the leaf length. **(E)** Length of *pMIR319C::GUS* domain relative to total leaf length in 50-350 µm leaf primordia are plotted for the indicated genotypes. N = 18-43. Significant differences among the samples are indicated by different alphabets. $p<0.05$. One-way ANOVA, followed by Dunnett's post hoc test are performed to determine the significant differences among samples.